AIAA 2002–1408

OPTIMIZATION OF PERFECT AND IMPERFECT RING AND STRINGER STIFFENED CYLINDRICAL SHELLS WITH PANDA2 AND EVALUATION OF THE OPTIMUM DESIGNS WITH STAGS

David Bushnell,* Fellow, AIAA, Retired
Charles Rankin, Associate Fellow, AIAA
Lockheed Martin Advanced Technology Center
Dept. L9-21, Bldg. 204, 3251 Hanover St., Palo Alto, CA 94304

ABSTRACT

Ring and stringer stiffened perfect and imperfect angle-ply cylindrical shells under combined axial compression and in-plane shear are optimized with a program called PANDA2 for the minimum weight design of stiffened panels, and the optimum designs are then evaluated with use of a general purpose finite element code called STAGS. The good agreement between PANDA2 and STAGS predictions for the nonlinear collapse of imperfect stiffened shells justifies the use of PANDA2 for preliminary design. A new PANDA2 processor called STAGSUNIT automatically generates STAGS input files for cylindrical panels and shells with both stringers and rings that have various open cross sections such as Blades, Zees, Jays, Tees and Is. In STAGSUNIT the edge conditions are formulated so that STAGS models of subdomains of a long cylindrical shell with many stiffeners can be constructed that do not have artificial prebuckling stress concentrations near the edges that might significantly affect predictions of bifurcation buckling and nonlinear collapse of the subdomain. Many STAGS models of optimized shells and subdomains of shells with Blade, Zee, and Tee stiffening are generated and explored, both with respect to linear bifurcation buckling and nonlinear collapse. The behavior of shells with an initial imperfection in the form of a general buckling mode of the imperfect shell is described from a physical point of view. Some difficulties encountered during this project are described.

INTRODUCTION

Purpose of this paper

The main purpose of this paper is to present minimum-weight designs derived by PANDA2 [1-10] for certain perfect and imperfect composite ring and stringer-stiffened cylindrical shells and to compare these with predictions from STAGS [11-13] for the optimized structures. PANDA2 and STAGS are described. A new PANDA2 processor called STAGSUNIT is described. STAGSUNIT automatically generates STAGS input files for ring and stringer stiffened panels and shells optimized by PANDA2. Although the development and analysis of optimum designs for which one or more of the design load combinations exceeds the local buckling load of the panel skin are within the scopes of both PANDA2 and STAGS, in this paper the stiffened shells are optimized such that local postbuckling deformation of the skin is not allowed in the PANDA2 models.

Brief review of the literature

Local and overall bifurcation buckling of stiffened panels can be determined with the BUCLASP code [14] and with the newer successors to BUCLASP and VIPASA: the PANDA2 [1-10], POSTOP [15], VICONOPT [16], and PASCO [17] codes. PASCO, VICONOPT, PANDA2 and POSTOP are capable of obtaining optimum designs of such panels, and PANDA2, POSTOP and VICONOPT can do so including the effect of local postbuckling [3] of the panel skin and/or parts of the stringers. One of the PANDA2 processors, called STAGSMODEL [4] automatically sets up a finite element model of a panel previously optimized with PANDA2. The [PANDA2, STAGSMODEL, STAGS] combination has been used many times to optimize and evaluate optimum designs of panels under combined loads for service in the postbuckling regime [3,4,8]. Other works are briefly surveyed in Ref.[16] cited in [8].

DESCRIPTION OF PANDA2

PANDA2 is a computer program for the minimum weight design of stiffened, composite, flat or cylindrical, perfect or imperfect panels and shells subjected to multiple sets of combined in-plane loads, normal pressure, edge moments, and temperature. For most configurations the panels can be locally postbuckled [3]. Previous work on PANDA2 is documented in [1-10]. PANDA2 incorporates the theories of earlier codes PANDA [2] and BOSOR4 [18]. The optimizer used in PANDA2 is called ADS [19]. Panels are optimized subject primarily to buckling and stress constraints.

PANDA2 processors and types of analysis

As described in [1-10], the PANDA2 system consists of several processors, BEGIN, SETUP, DECIDE, MAINSETUP, PANDAOPT, CHOOSEPLOT, CHANGE, STAGSMODEL, STAGSUNIT, etc. The functions of these processors are as follows:

BEGIN User establishes starting design, material properties, prebuckling and buckling boundary conditions.

SETUP System sets up BOSOR4-type templates for stiffness and load-geometric matrices.

DECIDE User chooses decision variables and bounds and sets up equality and inequality constraints.

MAINSETUP User chooses analysis type, loading, and solution strategies.

PANDAOPT Analysis type is performed (e.g. optimization).

CHOOSEPLOT User chooses what to plot.

DIPLOT The system obtains plots (postscript files).

CHANGE User changes selected variables and constants.

AUTOCHANGE A new starting design is automatically generated in a random manner.

SUPEROPT An attempt is made to find a global optimum design.

PANEL A BOSOR4 input file is generated for interring buckling of panel skin and stringers, with stringers modelled as flexible shell branches.

PANEL2 A BOSOR4 input file is generated for interring buckling of panel skin+smeared stringers with rings modelled as flexible shell branches.

STAGSMODEL An input file for STAGS [4,11-13] is generated (one finite element unit, only stringers are permitted).

STAGSUNIT An input file for STAGS is generated (multiple shell units, both stringers and rings are permitted).

CLEANPAN Delete all files except files containing user-provided input data for BEGIN, DECIDE, MAINSETUP, CHANGE, PANEL, PANEL2, STAGSMODEL and STAGSUNIT.

PANDA2 can be run in five modes:

1. Optimization
2. simple analysis of a fixed design
3. test simulation
4. design sensitivity
5. load-interaction (Nx,Ny), (Nx,Nxy), (Ny,Nxy)

Types of buckling included in PANDA2

PANDA2 computes general, inter-ring, and local skin buckling loads and mode shapes. General buckling is buckling in which both stringers (or isogrid stiffeners) and rings participate; "panel" (inter-ring) buckling is buckling between adjacent rings in which stringers (or isogrid stiffeners) participate but the lines of intersection of ring web roots with the panel skin do not translate; local buckling is buckling of the panel skin between adjacent stringers (or isogrid stiffeners) and rings. PANDA2 includes the following buckling models:

1. A discretized single skin-stringer module of the type shown in Fig.1 of [9], for example. This model is used for local buckling, local postbuckling, and wide column buckling of the panel region between adjacent rings (transverse stiffeners).

2. Simple models for the buckling of the panel skin and stiffener segments of the type described in [2]. Typical buckling modes of the panel skin and stiffeners are shown in Fig. 6 of [2]. In the panel skin the buckling nodal lines are assumed to be straight, as shown in Fig. 9 of [2]. This type of buckling model is used in some of the software written by Arbocz and Hol [20-22] and by Khot and his colleagues [23,24]. These models are

called "PANDA-type (closed form)" in PANDA2 jargon because they are the only ones used in the original PANDA program [2], which was superseded by PANDA2 [1] many years ago. Over the years an elaborate strategy has been developed in order to ensure that for each type of buckling in this "PANDA-type" category, the most critical (lowest) buckling load factor is not missed. The critical eigenvalue is determined from several searches over various regions in the (*m*,*n*,*slope*) domain, where *m* is the number of axial halfwaves, *n* is the number of circumferential halfwaves, and "*slope*" is the slope of the buckling nodal lines (non-zero when there is in-plane shear loading and/or shell wall anisotropy). More details are given in [10].

For sandwich panels and shells PANDA2 computes load factors for additional types of buckling that only occur for sandwich walls: face sheet wrinkling, buckling over the diameter of a single cell of a honeycomb core, and core crimping [7].

Three additional buckling models were recently added to PANDA2 as described in [9]:

3. Local buckling between adjacent stringers and rings of a cylindrical or flat panel obtained from a Ritz model in which the buckling modal displacement components, *u*, *v*, *w*, are expanded in double trigonometric series. The local region is assumed to be simply supported on all four edges.

4. General buckling of a cylindrical panel in which stringers and rings are treated as discrete beams with undeformable cross sections. Again, the general buckling modal displacement components, *u*, *v*, *w*, are expanded in double trigonometric series. The edges of the domain are assumed to be simply supported and to have discrete stiffeners of half the user-specified modulus. The domain for this model is a three-bay by three-bay subdomain of the entire panel.

5. A discretized single module model for a cylindrical panel in which the ring segments and panel skin-with-smeared-stringers are discretized as shown in Fig. 30 of [9]. Until the work leading to [9] was competed, the only discretized module model in PANDA2 involved the panel skin and STRINGER segments. The RINGS were "second-class citizens". In the discretized skin-with-smeared-stringers/ring "branched shell" model the cross sections of the rings can deform in the buckling mode, since they are subdivided into finite elements of the type used in BOSOR4 [18].

Buckling loads corresponding to a given type of buckling (such as local buckling of the skin between stringers or general buckling) may be computed by more than one model in order to verify results and to provide appropriate knockdown factors to account for anisotropy, inherent unconservativeness in smearing stiffeners, the presence of in- plane shear loading, and variation of in-plane loading within the domain that buckles. The effect of transverse shear deformation is accounted for as described in [1].

PANDA2 can optimize imperfect stiffened panels and shells [5]. The effects of initial geometric imperfections are described below.

Local post buckling analysis

An analysis branch exists in which local post buckling of the panel skin is accounted for [3,25]. In this branch a constraint condition that prevents stiffener pop-off is introduced into the optimization calculations [1]. The postbuckling theory incorporated into PANDA2 is similar to that formulated by Koiter for panels loaded into the far postbuckling regime [25].

Stress constraints

In addition to buckling constraints, PANDA2 computes stress constraints including local postbuckling deformations and thermal loading by both curing and applied temperature distributions. For laminated composite walls PANDA2 generates stress constraints corresponding to maximum tension along fibers, maximum compression along fibers, maximum tension transverse to fibers, maximum compression transverse to fibers, and maximum in-plane shear stress for each different material in a stiffened panel. For isotropic material PANDA2 generates stress constraints based on the von Mises effective stress.

Global optimizer SUPEROPT

Global optimum designs can be obtained with PANDA2 by means of a processor called "SUPEROPT", which is described in more detail in [6]. At intervals during the optimization process new "starting" designs are automatically generated as follows:

$$y(i) = x(i)[1 + dx(i)], \quad i = 1,2,..,N_D \qquad (1)$$

where N_D is the number of decision variables, $x(i)$ is the old value of the ith decision variable, $y(i)$ is the new value, and $dx(i)$ is a random number between -0.5 and +1.5 if the decision variable is other than a stiffener spacing and a random number between -1.0 and +1.0 if the decision variable is a stiffener spacing. The difference in treatment for decision variables that are not stiffener spacings from those that are stiffener spacings results from early experiments with SUPEROPT [6].

BRIEF DESCRIPTION OF STAGS

STAGS (Structural Analysis of General Shells), is a shell finite element program with a strong bias towards stability analysis capabilities [11-13]. Apart from having a good nonlinear shell modeling capability (small strain but arbitrarily large displacements and rotations), STAGS is also equipped with path-following techniques that make it possible to solve stability problems such as bifurcation buckling and collapse. The modeling capabilities include many design features that are frequently encountered in lightweight structures in the field of aero- and astronautics: a whole range of stiffener models, shell wall materials including composites, etc. In addition to the solution techniques for computing the static equilibrium branches of these models, STAGS also possesses robust transient time stepping methods.

PANDA2 PROCESSOR "STAGSUNIT"

Introduction

Most of the effort expended to produce this paper led to the creation of a new PANDA2 processor called STAGSUNIT. STAGSUNIT uses the PANDA2 database plus some interactive input from the user to produce the two input files for STAGS called *.bin and *.inp, in which "*" signifies the user-selected name for the case.

Table 1 lists typical input data for the new processor, STAGSUNIT. In this particular case the user is asking for an INDIC = 1 type of STAGS analysis (linear bifurcation buckling). Execution of STAGSUNIT produces the two STAGS input files, *.inp and *.bin. Table 2 lists the first part of the STAGS input file, *.inp in the annotated format automatically produced by STAGSUNIT. Table 3 lists the annotated *.bin file. Execution of STAGS followed by the STAGS postprocessor called STAPL produces plots of the type shown in Figs. 1 - 3. The STAGS input file, *.inp, is quite long. Table 4 lists just the headings in the *.inp file corresponding to Fig. 1, in which the cylindrical panel and all stiffener segments are modeled as shell units with 480 finite elements.

Scope of STAGSUNIT

STAGSUNIT works for cylindrical panels stiffened by stringers and/or rings with blade, T, I, J, or Z cross sections. Unstiffened panels can also be processed. The cylindrical panel can span less than 360 degrees of circumference, as shown in Figs. 1 - 3, or can form a complete (360-deg) closed cylindrical shell. The panel skin and various stiffener parts are modeled as (what is called in STAGS jargon) "shell units". All or parts of the stiffeners can be modeled as discrete beam elements (210 finite elements) or as shell units. The user has five choices with regard to each set of stiffeners, stringers and rings. For stringers, for example, the choices are identified in the PANDA2 PROMPT.DAT file [10] as follows:

> Stringer modeling index must be 1 or 2 or 3 or 4 or 5:
>
> 1 = all stringer segments are modeled as beams (210 elements) that are attached to the cylindrical shell.
>
> 2 = stringer webs are modeled as shell branches (410 elements) and any faying and/or outstanding flanges are modeled as beams (210 elements). The faying flanges are attached to the cylindrical shell and the outstanding flanges are attached at the tips of the stringer webs.
>
> 3 = all stringer segments (faying flange, web, outstanding flange) are modeled as shell branches.
>
> 4 = the stringer faying flange is modeled as a beam (210 elements), but the stringer web and stringer outstanding flange are modeled as shell branches.
>
> 5 = the stringers are replaced by enforcement of a constraint that the normal displacement w be constant along the generator where the stringer would be attached to the cylindrical shell. (NOTE: the correct prebuckling loading of the panel skin is used, that is, the actual stringers absorb their share of the prebuckling axial load.)

The same choices are provided in the modeling of rings.

Edge conditions

A large part of the effort of creating a reliable STAGSUNIT processor was spent on formulating proper edge conditions so that:

1. failure (bifurcation buckling and nonlinear collapse) as predicted from the STAGS model would probably not be in an "edge" mode induced by artificially introduced stress concentrations there, and
2. near-uniformity of the prebuckled stress state would be assured. (NOTE: the axisymmetric prebuckling "hungry horse" deformation caused by the rings [5] will still occur.)

In other words, failure would not be caused by one or more localized stress concentrations in the neighborhoods of one or more of the panel edges. The advantages of this favorable characteristic are:

1. The prebuckled state better simulates the model on which PANDA2 predictions are based, and

2. One can obtain similar results for subdomains of various sizes extracted from the full-sized panel or shell analyzed via PANDA2. There is a maximum numerical size of a STAGS model that can practically be processed. Therefore, one must often obtain predictions of failure from STAGS models that are based on a subdomain of the actual shell rather than on the entire shell.

Table 5 lists the part of the *.inp file (abridged to save space) concerned with edge conditions for STAGS models of the type shown in Figs. 1 - 3. The partial compatibility (g-2) record, "v=const", that is, constant circumferential displacement v along the curved panel edge at row 1 (x=0), permits uniform in-plane shear loading (torque) to be applied along row 1. The four "w=const" constraints along the four edges of the cylindrical panel eliminate any Poisson-ratio-induced nonuniformity in the prebuckling normal displacement field (w) in the neighborhoods of these edges. The contraints "ru=const" (no rotation about the generators) along row 1 (x=0) and row 41 (x=L) prevent numerical instability sometimes experienced in nonlinear STAGS runs when these constraints are omitted. The "w=constant" records for the stringer and ring faying and outstanding flanges help to prevent stiffener sidesway at the panel edges. The two sets of Lagrange constraints to prevent stringer and ring sidesway (only headings listed here to save space) force the webs of the stringers and rings to remain oriented radially at the edges of the panel. Even if stiffener sidesway is prevented, the outstanding flange is permitted to rotate in its plane, as can be seen at the ends of the stringers shown in Fig. 3. The four sets of Lagrange constraints to impose linear variation of axial displacement u and circumferential displacement v along the two straight edges permit uniform axial compression and in-plane shear loading along these two edges while generally preventing incremental buckling modal u and v components. The last five sets of Lagrange constraints are not present, of course, if the STAGS model is a closed (360-deg.) cylindrical shell.

Except in rare cases such as that shown in Fig. 4, these displacement constraints have the effect of causing the incremental bifurcation buckling modal displacement components u, v, and w to be zero along the panel edges where the constraints are applied. An exception is displayed in Fig. 4. The lowest buckling load for the axially compressed blade-stiffened cylindrical shell shown in Fig. 4 has a mode shape with the maximum normal modal displacement w at the boundary $x = L$. In this mode w is constant along the circumference at $x = L$. This “spurious” mode is avoided, as will be seen later, through the use of 480 finite elements with a sparser nodal point mesh near the boundary than in the interior of the shell. The mode is also avoided if, in his/her input to the STAGSUNIT processor, the user specifies that rings be located at the ends of the shell.

Along the curved edge at $x = L$ = XSTAGS the circumferential displacement v is fixed at zero. (See the second-to-last line of Table 5: "101 111" means all six displacement and rotation components are free except the circumferential displacement component v, which is held at zero both in the prebuckling and bifurcation buckling phases of the analysis.

Drilling freedoms suppressed

Table 4 lists many headings in the *.inp file containing the phrase, “drilling freedoms suppressed..” When the 480 finite element is used in a STAGS model, especially one involving nonlinear analysis, it is necessary to suppress the "sixth" nodal point degree of freedom: rotation about a normal to the shell. This "drilling" freedom should be suppressed everywhere except at nodal points where shell units intersect at some nonzero angle. Hence, when the user specifies use of the 480 finite element, drilling freedoms are suppressed in STAGS models generated via STAGSUNIT everywhere except where stiffener segments intersect each other or where they intersect the cylindrical skin at an angle other than zero. In a case with drilling freedoms not suppressed, the nonlinear STAGS analysis failed to converge for a load factor PA in excess of 0.137 With the same model with drilling freedoms appropriately suppressed, a converged stable equilibrium state was obtained by STAGS for a maximum load factor of about 0.95. (This example involved an axially compressed optimized perfect blade stiffened cylindrical shell with a very, very small "triggering" initial imper-

fection. PANDA2 predicted bifurcation buckling at a load factor of 1.0 and STAGS predicted linear bifurcation buckling at a load factor of 0.978. (See Fig.20.)

Various material, beam, and wall types

Almost half of the headings listed in Table 4 are concerned with the STAGS input libraries for material types (ITAM), beam cross section types (ITAB), and shell wall types (ITAW). These three libraries have two sections, one concerned with types not at an edge and the other concerned with types at an edge of the panel. In STAGSUNIT, stiffeners that run along edges are assigned materials with half the moduli and densities of the corresponding members that are not located at an edge. Because of this construction the behavior of a subdomain of the panel is permitted to behave in a manner similar to that of the entire panel.

For each stiffener there are three segments: the faying flange, the web, and the outstanding flange. Each of these segments is considered to be a separate discrete beam (210 elements used) and/or shell unit (410, 411, or 480 elements). Note: Only 410 shell elements can be used in the STAGS model if there exist in the same model discrete beams attached to the shell or to stiffener webs that are modeled as shell units.

Fasteners

In STAGS fasteners are like little springs that connect nodes across gaps in the finite element model. It is sometimes necessary to use fasteners in the STAGS models produced by STAGSUNIT because in optimum designs obtained by PANDA2 (especially for the cases that are the subject of this study), the heights of the stiffener webs are sometimes of the same magnitude as the thicknesses of the panel skin and faying flanges. Figures 2a,b show a STAGS model produced by STAGSUNIT in which fasteners are used. It can be seen, especially in Fig. 2b, that the gap between the stringers and the panel skin should not be neglected. This gap represents the thickness of the faying flange plus half of the thickness of the cylindrical skin. (The reference surface of the cylindrical skin is its middle surface in this case. See Fig. 5b.) In PANDA2 models the roots of the stiffener webs are assumed to be attached to the outer surface of the faying flange, as shown in Fig. 5a (except with Z-stiffeners, for which the web line of attachment is at the middle surface of the faying flange). The height H of the web is the distance from the root of the web to the middle surface of the outstanding flange. In the STAGS model shown in Fig. 2b, the short segments that represent the reference surfaces of the faying flanges of the stringers are located at the outer surfaces of these faying flanges (Fig. 5b).

If the user elects in STAGSUNIT not to include fasteners (see the appropriate entry near the bottom of Table 1), the outstanding flanges of the stringers and the web tips would have the identical locations of those shown in Fig. 2b, but the web would be extended radially inward to the reference surface of the cylindrical shell, as illustrated in Figs. 5c and 6. In such a case the user would select the outer surface of the cylindrical shell as the reference surface (provided the stringers are external). For external stiffeners STAGSUNIT would automatically select the inner surface of each faying flange as its reference surface, as shown in Fig. 6. This is done in order that all shell units are properly joined in the STAGS model, that is, there are no gaps where shell units are joined. STAGS does not permit gaps between shell units unless these gaps are "bridged" by fasteners, rigid links, or mounts.

Figures 5 and 6 display examples of fabrications and their STAGS models. Fig. 5b shows the STAGS model when the stiffener is attached to the panel skin with a fastener (actually, a "vector" of fasteners along the web root). Fig. 5c is the STAGS model when there are no fasteners, and Fig. 6 is the case where there are rings and stringers on opposite sides of the shell and no fasteners.

In the STAGS input file *.inp a library of fastener properties is included with the other libraries of materials, beam cross section properties, and shell unit wall properties. The fasteners themselves are entered as finite element units following data for all of the shell units. The PANDA2 processor STAGSUNIT always supplies just one entry in the library of fasteners: a spring with stiffness equal to six times the average of the axial and hoop stiffnesses of the panel skin. That is, the fastener spring constant equals $3(C_{11} + C_{22})$. Because of this relatively stiff spring the fastener acts in a manner similar to a rigid link. Rigid links were tried but were found to be unworkable in the present study because of conflict with certain of the edge and anti-sidesway conditions discussed in a previous subsection. Rigid links generate Lagrange constraints, some of which involve the same nodal points as the edge conditions. This duplication of Lagrange constraints generates ill conditioned equation systems. Fasteners do not generate any constraint conditions; they are simply additional parts of the structure and contribute to its strain energy. The numerical size of the STAGS model is much smaller when fasteners are used than when rigid links are introduced.

Choice of shell element (410 or 480)

In the writer's opinion (Bushnell) the most reliable finite element in the STAGS element library is the 480 [26] because buckling load factors from models constructed with this element almost always converge from above the "exact" value. Hence, it is almost always safe for the user to specify a low-density nodal point mesh in areas where he/she is not interested in obtaining local buckling behavior, such as near the panel edges in the cases studied here. Local buckling will occur first in areas of high nodal point density.

With use of the 410 element [27] this is not always true. Figure 7 shows an optimized, stiffened cylindrical shell. Nodal points are concentrated near the midlength of the shell. However for the applied load system (axial load Nx = -100 lb/in and in-plane shear load Nxy = +150 lb/in) STAGS finds local skin buckling everywhere EXCEPT where the nodal points are most concentrated even though the prebuckling resultants are uniform over the entire shell. This is not the kind of behavior that leads to practical (economic) and reliable predictions.

Unfortunately, as STAGS is currently written, it is not possible to attach discrete beam elements to a shell unit constructed of 480 elements. If 480 elements are used, all of the stiffener parts in each set (rings and stringers) must either be modeled as shell units or the stiffener set must be smeared out. Otherwise, the user must employ 410 elements.

APPROXIMATIONS USED IN PANDA2

Overall model

A complete cylindrical shell is modeled in PANDA2 as a panel that spans 180 degrees. The number of buckling halfwaves over 180 degrees is the same as the number of full circumferential waves in a closed cylindrical shell. If there is no in-plane shear or anisotropy and if the 180-degree panel is simply supported along its two straight edges, then predictions from the 180-degree panel would be exactly the same as those from a 360-degree (closed) model. The edge conditions for classical simple support are the same as those for antisymmetry. If in-plane shear Nxy and/or anisotropy are present, that is, if the buckling nodal lines have a non-zero slope, then the PANDA2 model represents an approximation.

Prebuckled state

1. The prebuckled state of a perfect cylindrical panel or shell is assumed to be the same as that for a complete (360-degree) closed cylindrical shell and is assumed to be axisymmetric; The stringers are "smeared" out in the prebuckling computations. Axisymmetric prebuckling bending caused by the presence of discrete rings ("hungry horse" deformation [5]) is retained in the PANDA2 model.

2. Prebuckling bending of an imperfect panel or shell with an imperfection in the form of the general buckling mode increases hyperbolically as the applied load is increased, approaching infinity as the applied load approaches the buckling load. (In PANDA2 the load-induced amplification factor applied to the initial imperfection amplitude is limited to 100 in order to avoid numerical instability.)

3. The "worst" (most destabilizing) stresses from imperfection-induced non-uniform prebuckling bending (such as ovalization) are assumed to be uniform over the entire shell in the bifurcation buckling phase of the computations. These imperfection-induced destabilizing prebuckling stress increments are superposed on the axisymmetric prebuckled stress state of the perfect shell.

4. Imperfection-induced prebuckling bending is assumed to occur without any local deformation of the cross sections of skin/stringer modules or skin-with-smeared-stringer/ring modules.

5. In an actual imperfect prebuckled shell, the circumferential radius of curvature varies over the shell. For example, in an ovalized cylindrical shell the circumferential radius of curvature varies as $\text{Amplit} \times \text{Wimp} \times \cos(2q)$, in which Wimp is the amplitude of the initial imperfection, Amplit is the amplification factor, greater than unity, from the hyperbolic increase of imperfection amplitude caused by the applied loads, and q is the circumferential coordinate. In PANDA2 the maximum circumferential radius of curvature at the given applied load is used as the "effective radius". This larger-than-nominal radius is assumed to be constant over the entire shell and is used in the bifurcation buckling analyses of the imperfect shell and subdomains of it that are required to obtain knockdown factors to account for the sensitivity of buckling loads to geometric imperfections.

6. Transverse shear deformation effects are not included in the prebuckling analysis.

Buckling analysis models with no discretization

1. The Ritz method with a limited number of terms is used to represent various modes of buckling [2,9].

2. In buckling of structural segments which are anisotropic and/or in which in-plane shear loading is present, the nodal lines of the buckle pattern can be "slanted", but these nodal lines are assumed to be straight (except in the "patch" models described below).

3. In computations of local buckling of the panel skin between adjacent stringers and rings and of local buckling of stiffener webs, simple support boundary conditions are assumed along the edges of whatever local domain is being analyzed, provided this local domain is bounded by other structure. For example, an outstanding flange occurs along one boundary of a stiffener web and the shell wall occurs along the opposite boundary. See Fig. 5 in [2] for an example of this type of local buckling of the segments of a stiffener.

4. In computations of local buckling of stiffener parts with one or more free edges, it is assumed that the cross section of that part of the stiffener does not deform in its buckling mode. It simply rotates about its line of attachment to other structure. The outstanding flange of a stiffener behaves in this manner. Also, the cross section of a blade stiffener simply rotates about its line of attachment to the faying flange or panel skin. The stiffener part is assumed to be simply supported along its line of attachment to other structure. For a blade stiffener, the number of halfwaves in the critical buckling pattern is assumed to be the same as that of the panel skin.

5. In stiffener buckling modes involving Tee- or Jay-shaped cross sections, there is a buckling mode in which the stiffener web and outstanding flange both participate. In this mode it is assumed that the line of intersection of these two stiffener parts does not displace. (Note, however, that this line of intersection DOES displace in the two stiffener rolling modes described in the next two items.)

6. In local buckling models of the panel skin in which rolling of the stiffeners is included, it is assumed that the cross sections of the stiffeners, while they can rotate about their lines of intersection with the panel skin, do not deform. See Fig. 6a in [2] for an example of this type of buckling.

7. In rolling ("tripping") analyses of a stiffener in which deformation of the web is permitted, the panel skin is assumed to remain undeformed and the deformation of the stiffener web is assumed to occur in a mode with a very small number of undetermined coefficients (Ritz method). The cross section of the outstanding flange does not deform. See Figs 6c,d in [2] for examples of this type of buckling.

8. There are two general buckling models that do not involve any cross-section discretization:

   a. General buckling of the entire panel or shell. In this model the stiffeners are smeared out in the manner of [28]. The nodal lines of the buckling pattern, while possibly slanted, must remain straight [23,24]. This Ritz model is described in [2].

   b. General buckling of a "patch" that includes nine bays, three in the axial direction and three in the circumferential direction. In this model, which is described in [9], the edges of the "patch" are assumed to be simply supported. Stiffeners are included both along the edges and in the interior of the "patch", but their cross sections, while rotating, are not permitted to deform in the buckling mode. The stiffeners along the edges of the "patch" have half the stiffnesses and densities of those in the interior of the "patch". The buckling deformations are expanded in a double trigonometric series with a limited number of terms [9].

9. In an analogous manner, there are two local buckling models that do not involve any cross-section discretization:

   a. Local buckling model analogous to (a) in the previous item. The nodal lines of the buckling pattern can be slanted but they must remain straight, as shown in Fig. 9 of [2].

   b. Local skin buckling model in which the edges of a single bay are assumed to be simply supported. The stiffeners, while they carry their proper share of prebuckling load, are neglected in the bifurcation buckling analysis. As with (b) in the previous item, the buckling deformations in the single bay are expanded in a double trigonometric series with a limited number of terms [9].

10. Obtaining buckling loads with smeared stiffeners is unconservative. Certain knockdown factors are computed in PANDA2 to compensate for this inherent unconservativeness of the "smeared" model. These are described in [10].

11. Transverse shear deformation effects are accounted for via a knockdown factor developed from a modified form of the Timoshenko beam theory, as described in [1].

12. In PANDA2, buckling is ALWAYS computed as a bifurcation phenomenon, never as a nonlinear collapse phenomenon. For example, in the case of general instability of an imperfect shell, PANDA2 computes the bifurcation buckling load factor of a panel the radius of curvature of which has been increased (hyperbolically) because of imperfection-induced prebuckling bending.

Buckling models with one-dimensional discretization

1. The "strip" method is used, that is, the discretization is one-dimensional. A single skin/stiffener module is included in the model, with symmetry conditions imposed midbay, as displayed in Fig. 1(b) of [9] for a skin/stringer module and in Fig. 30 of [9} for a skin-with-smeared-stringers/ring module. These one-dimensionally discretized module models are analogous to the model used in BOSOR4[18]. In fact, much of the coding from BOSOR4 (modified somewhat) is used in PANDA2. Variation of buckling modal displacements in the coordinate direction normal to the plane of the discretized module cross section is assumed to be trigonometric, with wavelength specified by the number of halfwaves in the buckling pattern over whatever domain governs (*e.g.* distance between adjacent rings for the discretized skin/stringer module model and circumferential length of the panel for the discretized skin-with-smeared-stringers/ring module model).

2. Previously in PANDA2 the discretized skin/stringer module model did not include the curvature of the panel. The optimized configurations developed during the effort required to produce this paper have dimensions that render the "flat" discretized module model too conservative. Therefore, PANDA2 was improved. The PANDA2 user can now choose whether or not to retain the curvature of the panel skin in this model. The results in this paper were obtained with use of the curved discretized skin/stringer module model in PANDA2 analyses.

3. The effects of in-plane shear loading Nxy and/or anisotropy are included indirectly. Buckling loads and mode shapes from the discretized module models are determined neglecting these effects, since the BOSOR4 model was never able to include them. Then a knockdown factor computed from the non-discretized models described in the previous subsection is generated. This knockdown factor is computed by PANDA2's running two local buckling analyses with the non-discretized (PANDA-type[2]) models:

   a. A local skin buckling analysis in which in-plane shear and anisotropy are included,

   b. A local skin buckling analysis in which in-plane shear and anisotropy are neglected.

   The knockdown factor to account for in-plane shear Nxy and/or anisotropy is the ratio, a/b, of the two local buckling load factors.

4. In the local postbuckling analysis (the KOITER branch of PANDA2 [3], not used in the study described in this paper) a starting value of the slant of the buckling nodal lines is obtained from the non-discretized model for local buckling. The initial mode shape for local postbuckling deformations is that obtained from the discretized skin/stringer module model with a flat skin. The postbuckled equilibrium state is obtained from a system of nonlinear algebraic equations in which the unknowns are the amplitude of local postbuckling displacement of the panel skin midway between stringers, a "flattening" parameter which is a measure of the deviation of the local postbuckling pattern from pure sinusoidal, the slope of the local postbuckling nodal lines, and the halfwavelength of the local postbuckling pattern in the direction parallel to the stringers. Details are given in [3]. The postbuckling model is based on the assumption of an initially flat panel skin.

5. The effect of transverse shear deformation is accounted for via a knockdown factor as described in the previous subsection.

Effect of imperfections on buckling

1. The presence of initial geometric imperfections has two consequences:

   a. The prebuckling stress state changes because the imperfect shell bends as soon as any load is

applied.This causes stresses to be redistributed among panel skin and stiffener segments (faying flange, web, outstanding flange). The redistribution of prebuckling stresses of course affects local buckling loads of the various stiffener parts, local buckling of the panel skin, and lateral-torsional rolling of the stiffeners.

b. The radius of curvature of the panel increases in some areas and decreases in other areas. The PANDA2 models neglect any decrease and always use the largest radius of the deformed panel in the various bifurcation buckling analyses.

2. The effect of stress redistribution is approximated as described in the subsection above on prebuckled state.

3. Knockdown factors for general, inter-ring, and local buckling are computed from the nondiscretized models described above. Buckling load factors are first obtained for the perfect panel. Then a new (larger) radius of curvature is computed from the assumption that this radius grows hyperbolically with increase in ratio of applied load to buckling load of the imperfect shell. A new buckling load is computed. Iterations continue until convergence is achieved. The knockdown factor is the ratio of the buckling load factor of the shell with the larger, converged, radius of curvature to that of the perfect shell. The buckling modal imperfection shape used in PANDA2 for buckling and stress analysis is that corresponding to the deformed shell, that is, the shell with the larger, converged, radius of curvature. In this phase of the computations redistribution of the prebuckling stresses due to imperfection-induced prebuckling bending is not included. The knockdown factors reflect only the effects of change in geometry due to the initial buckling modal imperfection as amplified by the applied loads. The effect of the stress redistribution during imperfection-induced prebuckling bending is accounted for in other sections of the PANDA2 code because the locally increased destabilizing stress resultants are used in the various local buckling, postbuckling and stress analyses of the perfect structure.

4. Another set of knockdown factors for general, inter-ring, and local buckling is computed from part of Arbocz' theory as described in [6,20]. This is the part of Arbocz' theory analogous to Koiter's special theory [29]. Koiter's special theory yields buckling knockdown factors for axially compressed monocoque cylindrical shells based on the assumption that the initial imperfection is axisymmetric and varies sinusoidally in the axial direction with an axial wavelength equal to that of the axisymmetric buckling mode of the perfect shell. The decrease in buckling load from that of the perfect shell is caused by induced hoop compression in circumferential bands where the generator of the imperfect shell is bowed inward axisymmetrically. Arbocz [20] extended the Koiter special theory to handle cylindrical shells with a general orthotropic 6 x 6 constitutive matrix.

5. For each type of buckling (general, inter-ring, local) PANDA2 uses the minimum knockdown factor from the theory with hyperbolically increased radius of curvature and from Arbocz' theory.

Miscellaneous approximations

PANDA2 computes stress and buckling margins corresponding to two locations along the axis of a ring-stiffened panel: 1. midway between rings, called "Subcase 1" and 2. at the ring stations, called "Subcase 2". Prebuckling conditions are different at these two locations because of the axisymmetric "hungry horse" deformation caused by the rings (described in [5]). General instability calculations and the calculations involving the three-bay by three-bay "patch" model [9] are performed only for Subcase 1. If there exists an initial general buckling modal imperfection, PANDA2 employs the user-supplied amplitude of it in the Subcase 1 computations and the negative of that amplitude in the Subcase 2 computations. The prebuckling stresses that exist at each of the two locations are assumed by PANDA2 to be uniform over the entire shell during the bifurcation buckling phase of the analysis.

Margins for an optimized design of a Z-stiffened shell

Table 6 lists all the margins computed for one load case and one of the two subcases for that load case. (Subcase 1 corresponds to conditions midway between rings and Subcase 2 corresponds to conditions at a ring station.). The data in Table 6 are for an optimized imperfect 4-layered angle-ply cylindrical shell stiffened by rings and stringers of orthotropic material with Z-shaped cross sections. The shell is subjected to a combination of uniform axial compression, Nx = -700 lb/in and in-plane shear, Nxy = +40 lb/in. (See Tables 7 and 8 for specifics about the optimum design.)

Margins 1–11 in Table 6 are generated from discretized single module models and Margins 12–37 are

generated from models with no discretization. There are many stress constraints because each layer of the panel skin and each stiffener segment are orthotropic. Each of the two orthotropic materials has associated with it five stress allowables and therefore generates five stress constraints: maximum tension along fibers, maximum compression along fibers, maximum tension normal to fibers, maximum compression normal to fibers, and maximum in-plane shear stress. (Material 1 is used in the panel skin, and Material 2 is used in all the stiffener parts.) In this particular case none of the stress constraints is critical for the optimum design. The shell is lightly loaded. Local postbuckling is not permitted. (The factor of safety for local buckling is 1.0.) Therefore the optimum design is governed by buckling constraints, not stress constraints. The most critical margins are Margins 1, 2, 10, 11, 28, 29, and 30, all buckling margins.

More than one margin listed in Table 6 may represent a different model of approximately the same physical behavior. For example, Margins 2, 10, and 32 may all represent different models of lateral-torsional buckling of a stringer with and without participation of the panel skin. Margins 1, 2, and 28 all represent different models of local buckling of the panel skin between adjacent stringers and rings. Margins 1 and 2 include rolling of the stringer cross section and Margin 28 does not. Margins 11 and 30 may both represent buckling of a bay between adjacent rings with little or no participation of the rings in the buckling mode. It turns out that for all the cases studied here Margin 30, although defined as a form of "general buckling", is primarily inter-ring buckling or local buckling. (Margin 30 is generated from the three-bay by three-bay model mentioned above and described in detail in [9]. It turns out that, of all the coefficients of the double trigonometric series expansion of the buckling mode, the coefficients corresponding to m = 3 axial, n = 3 circumferential halfwaves are the largest in most of the cases studied here.)

The string "SAND" in Margins 28–37 means that Sanders' shell theory [30] was used to obtain the buckling predictions.

The precise meaning of many of the margins listed in Table 6, especially those regarding buckling of stiffeners and parts of stiffeners, are given in [6].

From the long list of margins, each one representing a possible mode of failure of the structure, it is seen that the philosophy used in PANDA2 is to examine many different phenomena separately, each one in an approximate manner in an attempt to obtain reasonable optimum designs for which no mode of failure has inadvertently been overlooked. In PANDA2 a very complex problem is divided into many relatively simple parts. Because each part is numerically small, cases run fast on the computer. The PANDA2 modeling is therefore ideal for use with optimization. Many assumptions and approximations are made in the process. Therefore, the suitability of the optimum designs obtained by PANDA2 must be checked by exercising a more general and more rigorous analysis such as that embedded in the STAGS computer program [11–13].

The philosophy in STAGS is to permit the high-fidelity analysis of a complex structure which may exhibit complex nonlinear behavior. The failure of the structure as predicted by STAGS may represent some combination of the several possible failure modes examined in many separate analyses in PANDA2. The main purpose of this paper is to determine if, for the cases studied here, the optimum designs developed by PANDA2 are safe but not overly conservative, according to predictions by STAGS.

RESULTS FROM PANDA2

Introduction

Optimum designs of perfect and imperfect cylindrical shells stiffened by rings and stringers with Blade, Tee, and Zee cross sections are found with use of PANDA2 then analyzed with STAGS. In the cases studied here both rings and stringers always have the same type of cross section (Blade, Tee, Zee) and the stringers are always external and the rings internal. All stringers are the same and all rings are the same. The cross section dimensions of a stringer may be different from that of a ring. Note that the case called "Tee" might well have been called "I", since the Tee stiffeners have faying flanges. The term "Tee" is used here because that is the nomenclature used in PANDA2. Unlike the Tee stiffeners and the Zee stiffeners, the Blade stiffeners have no faying flanges in the cases studied here.

Table 7 lists the names and definitions of all the variables that may change during optimization cycles (decision variables and linked variables). Table 8 lists the values of the variables before and after optimization and also gives other data pertaining to all cases.

The lower and upper bounds of stringer spacing B(STR) and ring spacing B(RING) are set so that if the optimum design corresponds to bounds of these variables there will be an integral number of equally spaced stiffeners in the complete (360-deg.) cylindrical shell of length 60 inches and radius 6 inches. The STAGSUNIT processor is programmed so that if a user supplies a circumferential length (called L2 in the

prompt in Table 1, "Panel length in the plane of the screen, L2", and called YSTAGS in STAGSUNIT and Y in some of the tables) that is less than 80 per cent of that corresponding to the complete (360 deg.) cylindrical shell, STAGSUNIT changes the user's input so that the circumferential length Y used in the STAGS model is equal to an integral number of stringers with spacing equal to the value B(STR) in the PANDA2 data base. If the user supplies an "L2" that is greater than 80 per cent of 360 degrees of circumference, STAGSUNIT sets L2 equal to $2\pi r$. The axial length supplied by the user in STAGSUNIT is treated differently. STAGSUNIT does not change the user's input but changes the ring spacing B(RNG) to one in which an integral number of rings fits into the length XSTAGS supplied by the user. If this new spacing is significantly different from the PANDA2 value B(RNG), STAGSUNIT prints a warning message. The original value of B(RNG) in the PANDA2 data base remains unchanged after completion of the STAGSUNIT process.

Results were first obtained for the Blade stiffened perfect and imperfect cylindrical shells. It was difficult to find global optimum designs, especially for the imperfect shell, for a reason that will be explained in the next subsection. However, after many, many executions of the global optimizer SUPEROPT, it was found that the minimum-weight design corresponds to that with both the stringer and ring spacings at their lower bounds, 1.885 in. and 4.0 in., respectively. Therefore, in the runs involving Tee and Zee stiffeners the stringer spacing was fixed at B(STR) = 1.885 in. and the ring spacing was fixed at B(RNG) = 4.0 in.

Results for all cases are listed in Tables 8 - 18. Typical models and predictions from PANDA2 and STAGS are displayed in Figs. 8 –40.

Results from PANDA2

Results from PANDA2 are listed primarily in Tables 8 - 12. Plots generated by means of the PANDA2 processors, CHOOSEPLOT and DIPLOT, appear as Figs. 8 - 15. All of these figures apply to the blade stiffened option.

Optimization of the perfect Blade stiffened shell

Figure 8 shows the objective (objective = weight of 180 degrees of the cylindrical shell) vs design iterations during the first execution of the global optimizer, SUPEROPT. Each relatively high spike in the plot represents a new "starting" design generated by AUTOCHANGE [6]. In this execution of SUPEROPT the user specified that PANDAOPT be executed five times after each execution of AUTOCHANGE. SUPEROPT keeps running as long as the total number of design iterations is less than 270.

Before this execution of SUPEROPT the user chose a modeling index, IQUICK=1 in the MAINSETUP processor. With IQUICK = 1 the discretized skin-stringer module model is not used [1].

The spacings of the stringers and rings were permitted to vary between the bounds listed near the bottom of Table 8. The minimum weight for an “ALMOST FEASIBLE” design was 2.12 lbs. after completion of the run. (As explained in previous papers on PANDA2, the PANDA2 optimizer terms a design for which any margin is less than -0.05 as “UNFEASIBLE,” a design for which all margins are greater than -0.05 but some margins are less than -0.01 as “ALMOST FEASIBLE,” and a design for which all margins are greater than -0.01 as “FEASIBLE”. PANDA2 accepts “ALMOST FEASIBLE” designs.)

Results from another execution of SUPEROPT are shown in Fig. 9. In this case the spacings of the stringers and rings were fixed at B(STR)=1.885 and B(RNG) = 4.0 in., respectively, and the modeling index IQUICK = 0. The user chose to retain the curvature of the shell in the discretized single module model [10]. SUPEROPT produced essentially the same optimum design of the perfect shell as that produced by the run with IQUICK=1.

Figure 10 displays the most critical margins (generated during the execution of SUPEROPT with IQUICK = 0) corresponding to Load Set # 1, (Nx,Nxy) = (-700, +40) lb/in, and Subcase 1, conditions midway between rings. (Conditions at midbay are different from those at the ring stations because of "hungry horse" prebuckling axisymmetric bending [5].) It is hard to see which of the margins governs the evolution of the design because the plot is so crowded.

However, the most critical margin names for all cases are listed in Table 9, and Tables 10 and 11 give the values of these for Load Set 1 and Load Set 2, respectively, corresponding to the optimum designs for all cases. For the perfect Blade stiffened cylindrical shell and for Load Subcase No. 1, Margins 1, 11, 12, 13, and 21 are critical or nearly so, and Margins 2, 4, 18, and 20 are all less than 0.4. For the perfect Blade stiffened shell and for Load Subcase 2, Margins 1, 2, 3, 4, and 11 are critical or nearly so, and Margin 7 is less than 0.4. The optimum design is "ALMOST FEASIBLE" because Margin 2 for Subcase 2 is -.048. There are fewer critical and almost critical margins for

Load Set 2, the load set in which the shell is under much more in-plane shear, Nxy. These are listed in Table 11. Note that the margin definitions in Table 9 contain strings such as "M=9", m=2, "M=1;N=2", "slope=100.", "z=0.0125", etc. In the different cases these values will be different. Consider Table 9 to be a sample only. The types of buckling remain the same but the numbers of halfwaves, slope of buckling nodal lines, coordinate z through the thickness, etc. will change from case to case.

Optimization of the imperfect Blade stiffened shell

An imperfection in the shape of the general buckling mode is introduced into the PANDA2 model. The amplitude of the imperfection is Wimp = 0.025 in.

Figure 11 shows the results of one of many (26) SUPEROPT runs executed to get the global minimum-weight design. In all runs the stringer and ring spacings were fixed at B(STR) = 1.885 in. and B(RNG) = 4.0 in., respectively. PANDA2 has a hard time finding the global optimum as can be seen from the "jumpy" nature of the plot in Fig. 11. The minimum weight, 2.548 lbs for 180 degrees of the shell, is very close to the minimum value reached in Fig. 11 just before 100 iterations. During the many SUPEROPT runs PANDA2 found that minimum rarely, less than once on average for each execution of SUPEROPT.

In order to find out why the plot in Fig. 11 is so "jumpy", a single PANDAOPT execution was made with 20 design iterations, as shown in Fig. 12. Prior to this execution the input file for the PANDA2 processor DECIDE was changed by putting very tight bounds on the decision variables and DECIDE was rerun. The starting design is the optimum design with weight 2.548 lbs. Figure 12 shows the objective and Fig. 13 the margins for Load Set 1, Subcase 1. Note that the most critical margins, “simple support local buck.” and “rolling with local buck.” are oscillating with almost every iteration. The objective (Fig. 12) drifts above the optimum weight, 2.548 lbs.

The results listed in Table 12 help to reveal what is happening. Table 12 gives general instability load factors for an imperfect shell (shell with a larger radius than the nominal radius of 6.0 in.) from the PANDA-type model (nondiscretized model [2,10]) for three designs that are very close to eachother. For each of the three neighboring designs, six eigenvalues (general buckling load factors) and corresponding mode shapes (*m,n,slope*=axial halfwaves, circumferential halfwaves, slope of the buckling nodal lines) are given. These are the results of a search by PANDA2 over six regions in (*m,n,slope*) space in order to determine the lowest (most critical) load factor and mode shape [10].

Note that for each of the three neighboring and nearly optimum designs, the mode shapes corresponding to the most critical general buckling load factor are very different. For the first design (the optimum design determined after all those executions of SUPEROPT), the critical load factor and mode shape are 2.08(1,4,0.228). For the second and third neighboring designs the critical values are 2.32(7,5,0.) and 2.27(10,6,0.), respectively.

Remember that PANDA2 uses the general buckling mode (*m,n,slope*) of the imperfect shell in order to determine the effective radius of the loaded, imperfect shell and to determine the redistribution of prebuckling stress resultants and stresses caused by prebuckling bending of the imperfect shell. The amount of prebuckling bending will differ considerably for the three different critical modes of the three neighboring designs. The modes with the highest number of axial and circumferential halfwaves will cause much greater curvature changes and hence much greater additional destabilizing prebuckling stresses in the various stiffener segments and panel skin than that with the fewest number of waves. It is primarily the local buckling margins that are affected by stress redistribution and change in the effective circumferential radius of curvature. The effective radius of the panel skin is greatest for the third design, for which there are the highest number of circumferential halfwaves in the critical general buckling mode (n = 6).

From design iteration to iteration the mode shape for general buckling of the imperfect shell oscillates from the relatively long-wavelength mode of the type displayed for the first design to the shortest-wavelength mode of the type displayed for the third design. This abrupt switching of the critical general buckling mode shape from iteration to iteration causes the dramatic oscillations of the local buckling margins shown in Fig. 13 and makes it very difficult for PANDA2 to find global optimum designs of the imperfect shell in this particular case.

Figure 14 demonstrates the same problem in a different type of PANDA2 analysis: sensitivity of the optimum design of the imperfect Blade stiffened cylindrical shell to changes in the height H(STR) of the stringers. The optimum design of the imperfect Blade stiffened shell is listed in Table 8. There, the optimum stringer height is given as H(STR)=0.2272 in. It is seen from Fig. 14 that for H(STR) slightly less than the optimum value there is a large jump in the two local skin buckling margins and a smaller jump in the

buckling margin for "stringer seg. 3" (PANDA2 jargon for the web or Blade stiffener in this case). At the top of the jump the general buckling mode shape of the imperfect shell has the mode shape corresponding to the first design of Table 12. At the bottom of the jump, where the local buckling margins are significantly negative, the imperfect shell has the mode shape corresponding to the third design of Table 12. The design sensitivity is essentially infinite at the jump. The very large gradients in buckling behavior there make it difficult for PANDA2 to find the global optimum design.

Load interaction curve, Nx(crit) vs Nxy(crit)

Figure 15 shows load-interaction curves generated by PANDA2 for the optimized imperfect Blade stiffened shell for the margins listed in the legend. The two sets of applied loads, $(Nx,Nxy)_1 = (-700,+40)$ lb/in and $(Nx,Nxy)_2 = (-100,+150)$ lb/in, are included in the figure as two points. These two points, somewhat hard to see, fit just inside the interaction curves nearest the origin, as is to be expected. The most sensitivity to the initial general buckling modal imperfection with amplitude Wimp (general) = 0.025 in. is exhibited by the two curves for local buckling. The reduction in capacity from the corresponding curves for the perfect shell is due to the redistribution of compressive membrane prebuckling stress resultants to the panel skin and to the increase in effective circumferential radius of curvature of the cylindrical shell both initially and as it bends under the applied loads.

Discussion of PANDA2 results for all cases

The PANDA2 predictions for all cases are listed in Tables 8 - 11. The following points pertain to the results in Table 8:

1. The layup angle ANG of the angle ply, $[ANG, -ANG, -ANG, ANG]_{total}$, approaches its upper bound, 70 degrees, in all cases. Given the two load sets, $(Nx,Nxy)_1$ and $(Nx,Nxy)_2$, the best design for both the perfect and imperfect shells is one in which at least 87 per cent of the axial load is carried by the stringers. (The case for which the skin carries the highest percentage of the axial load is the optimized perfect shell with the Blade stiffeners.)

2. The thicknesses of all segments of the rings approach the lower bound of 0.03 in. For the imperfect shell with the Tee stiffeners, the widths of all the ring segments are essentially at the lower bound of 0.10 in.

3. The Blade stiffened shells are the lightest. However, this may be an artifact of lower bounds on stiffener segment dimensions that are set fairly high.

4. For all the optimized perfect shells and for the imperfect shell with Zee stiffeners the heights H(STR) of the stringers are not large compared to the thickness of the skin plus stringer faying flange. This geometry may lead to the requirement that fasteners be used in the STAGS models in order to permit proper modeling of the junction between the stringer root and reference surface of the cylindrical shell. Figures 5 and 6 shows how the STAGS models are constructed with and without fasteners. If one of the critical or nearly critical types of buckling includes rolling of the stringers in a lateral-torsional mode, then the no-fastener STAGS model that requires extension of the web through the faying flange to the surface of the cylindrical shell, as shown in Figs. 5c and Fig. 6, may lead to overly conservative predictions of bifurcation buckling and collapse in the lateral-torsional mode.

5. The optimum cross sections of the stringer faying flanges, especially for the perfect and imperfect shells with Zee stiffeners and the imperfect shell with Tee stiffeners, are not really practical, being too "square". Probably a smaller upper bound should have been used for the thicknesses of these stringer parts.

The following points pertain to the results in Tables 10 and 11:

1. The most consistently critical margin for all cases, both for Load Set 1 (Table 10) and Load Set 2 (Table 11), is Margin No. 11, “simp-support local buck.; (0.95*altsol)...”. This margin is computed via the alternate double trigonometric series expansion solution (hence the string "altsol") described in [9]. The string "local buck." Refers to local buckling of the panel skin. The stringers and rings are neglected in the bifurcation buckling phase of the computations. (They absorb their share of the prebuckling load, however.) The four edges of the local domain, that is, the domain bounded by adjacent stringers and rings, are assumed to be simply supported in the bifurcation buckling phase of the analysis. In general, this may or may not be a conservative model. It depends on whether the dimensions are such that stiffener rolling forces the skin to buckle (stiffen-

ers too weak relative to the skin) or whether the stiffeners help to prevent rotation of the skin about its edges (stiffeners too strong relative to the skin). In all the cases run here the "altsol" model of local buckling turns out to be conservative, especially for Load Set 2 (applied in-plane shear dominates) in which the stiffeners are not heavily loaded in axial compression.

2. Margin 13 is often critical or nearly so in Load Set 1. This margin is computed from the three-bay by three-bay "patch" model discussed previously and described in detail in [9]. Although the string, "general buck.", occurs in the identifying phrase for Margin 13, it turns out that in the cases studied here the buckling mode derived from this model resembles buckling between adjacent rings and stringers (a form of local buckling) because the trigonometric terms with $m = 3$ axial halfwaves and $n = 3$ circumferential halfwaves over the "patch" dominate the double trigonometric series expansions for the normal displacement (w) field.

3. Margin 4, "Inter-ring buckling, discrete model..." is often critical in Load Set 1. This margin is computed from the discretized skin-with-smeared-stringers/ring module model mentioned above and described in detail in [9]. It is a PANDA2 model in which deflection normal to the panel skin at the ring web root is prevented and symmetry conditions are imposed midway between rings. (See Fig. 30 of [9]).

4. Margin 21 only applies to the shells with Blade stiffeners for which there are no faying flanges in the particular cases studied here. In the PANDA2 processor BEGIN the user is forced to supply a non-zero value for the width B2(STR) of the base under the stringer, even if there is no faying flange there. When there is no stringer faying flange and when the discretized skin-stringer module model is used (IQUICK=0), it is advantageous from a numerical point of view to force the width of the stringer base always to be approximately one third the spacing B(STR) between stringers as the cross section evolves during design iterations. There is an internal inequality constraint imposed by PANDA2 that the stringer base must not exceed one third of the stringer spacing. In the cases studied here involving Blade stiffeners a linking constraint is introduced by the user during processing with DECIDE: The stringer base must always equal 0.3333 times the stringer spacing. Hence, Margin 21 is always critical for the cases involving Blade stringers. It does not effect the evolution of the design, however.

RESULTS FROM STAGS

Introduction

The various STAGS models of the perfect and imperfect panels optimized by PANDA2 are identified in Table 13. All of these models except Model "0" are generated by execution of the new PANDA2 processor STAGSUNIT. Table 14 lists the types of buckling observed to occur. Sometimes it is necessary to specify "2,3" if skin buckling and stiffener rolling appear to play approximately equal roles in the buckling pattern. Similarly, a specification "4,5" indicates a mode which appears to be the average of "4" and "5". Occasionally, a specification such as "2,3,4" is appropriate.

The STAGS predictions for bifurcation buckling and collapse are listed for the Blade stiffened panels and shells in Tables 15 and 16, for the Tee stiffened panels and shells in Table 17, and for the Zee stiffened panels and shells in Table 18. Tables 16 - 18 are divided into three categories from top to bottom:

1. buckling of the optimized perfect shells
2. buckling of the optimized imperfect shells treated as if they were perfect
3. buckling of optimized imperfect shells with non-zero amplitudes for imperfections in the shapes of buckling modes.

The STAGS predictions listed under the third category, perhaps the most important in this paper, are loads at which a nonlinear STAGS analysis indicates collapse occurs for an initially imperfect shell.

Also listed in Tables 15 - 18 are buckling load factors from PANDA2. These predictions appear on the right-hand halves of the tables near the top of each of the three categories. They are listed under the five headings, "Stringer segment", "Lateral torsion", "Local skin", "Inter-ring" and "General buckling". For each of the two load sets, called "Load 1" and "Load 2" in Tables 15 - 18, the values listed correspond to the lowest predictions from either Subcase 1 (conditions at midbay) or Subcase 2 (conditions at rings). Note from Tables 9 – 11 that there are more than five buckling margins from PANDA2. For each of the two load sets the writer (Bushnell) selected the smallest margin that would fit into one of the five headings. For example, under "Inter-ring" are mostly listed the smallest of Margins 13 (Table 9) from Subcase 1 and Subcase 2. This is because Margin 13, based on the three-bay by

three-bay "patch" model [9], captures a buckling mode that is primarily inter-ring or local buckling rather than general buckling in the particular cases investigated here. Also, often listed under "Lateral-torsion" are the smallest of Margins 2, "Long-wave local buckling, discrete model", from Subcase 1 and Subcase 2 because this type of buckling often resembles a lateral-torsional stiffener rolling mode with participation of the panel skin. The buckling load factors from PANDA2 listed in the first (top) and third (bottom) categories in Tables 16 - 18 can be obtained from the margins listed in Tables 10 and 11 by adding one to the appropriate margins. Table 9 must be used to obtain the definition of the margin. In this way the reader can determine exactly what kind of buckling corresponds to the PANDA2 buckling load factors selected for listing in Tables 16 - 18.

In Tables 15–18 *n* is the number of circumferential halfwaves and *m* is the number of axial halfwaves in whatever domain is being considered. *n* is the number of circumferential halfwaves in the 180-degree PANDA2 model and *n* is the number of full circumferential waves in the STAGS model of the closed (360-deg.) cylindrical shell.

One can see examples of the various STAGS models and various types of buckling in Figs. 16 –26. Figures 16 a-c show buckling of the skin in one 4.0 x 1.885 inch bay. The stringers and rings have been replaced by constraints that the normal buckling modal deflection *w* be constant along all four edges. Figures 16 d–f show buckling of one bay in which stiffeners with half the nominal stiffness and density are located along the four edges. The models depicted in Figs. 16 are all of type “1” in Table 13. Figure 17 shows skin buckling in a STAGS model of type “2.” Figure 18 shows an example of STAGS model type “3” for which the lowest buckling load has a mode which is primarily inter-ring buckling with major deflection of some of the stringer roots, that is, buckling mode type “5” listed in Table 14. Figure 19a shows a STAGS model type “4” with a buckling mode that might be considered an “average” of buckling types “2” and “3” in Table 14. Figure 19b displays the mode of collapse of the same Tee stiffened shell with a buckling modal imperfection with shape given in Fig. 19a and with initial amplitude of 0.01 in. The mode of collapse is more of type “2” in Table 14 than of type “3.” Figures 20 - 22 show the lowest buckling mode of a Blade stiffened shell with use of STAGS model type “5” in Table 13. The buckling mode is of type “5” in Table 14. Strictly-speaking, the buckling mode shown in Figs 20 - 22 is a type of general instability because the roots of the ring webs deflect in the radial direction, as shown in Fig. 22. However, comparison of Figs. 21 and 22, which are plotted to the same scale, demonstrate that the amplitude of the ring deflection is far less than that of the shell midway between rings. Figures 23, 24 and 25 all show examples of STAGS model type "5", with buckling of types "6", "7" and "8", respectively. Figure 26 shows a STAGS model type "3" with buckling of type "9".

In the writer's opinion (Bushnell) the most significant results of this study are listed under the third category (bottom) of Tables 16 - 18. These are collapse loads of imperfect cylindrical shells optimized by PANDA2. PANDA2 predicts failure of such shells at a load factor very close to unity. The collapse load factor predicted by the best STAGS models varies from a low of about 0.92 for the Tee stiffened shell to a high of about 1.09 for the Blade stiffened shell.

Results from STAGS for the Blade stiffened shells

Tables 15 and 16 contain the predictions.

Table 15 pertains to local buckling of the panel skin between adjacent stiffeners. The best STAGS model for skin buckling of the stiffened shell is that of type "2", shown in Fig. 17. The STAGS predictions are about 18 per cent above the PANDA2 prediction of skin buckling for Load Set 1 and about 30 per cent above the PANDA2 prediction for Load Set 2. Most of the difference is caused by the presence of the stiffeners in the STAGS model. In this case the stiffeners, according to the STAGS prediction, help the skin to resist buckling. The STAGS model of skin buckling that is closest to the PANDA2 model is that of type "0". For that model STAGS and PANDA2 yield buckling load factors for skin buckling within about 5 per cent of eachother for both load sets. The model leading to the lowest STAGS prediction for skin buckling, 0.831, allows the two straight edges to undergo in-plane warping both in the prebuckling and bifurcation phases of the analysis. The prebuckled state of prestress is significantly nonuniform. This unrealistic condition also exists for the model associated with the skin buckling load factor 0.974. The model leading to the second lowest STAGS prediction, 0.957, yields a peculiar buckling mode. It is essentially the same as that shown in Figs. 16a and 16c. Note from Fig. 16c that there exists a uniform normal buckling modal displacement *w* along the four edges of the panel, a buckling modal deformation permitted by the STAGS models generated via the PANDA2 processor STAGSUNIT, but not likely to occur in an actual structure because of edge restraint provided by stiffeners. Fortunately, this “spurious” mode is rare and can easily be

avoided through the use of STAGS models with stiffeners along the edges.

Table 16 lists buckling predictions from PANDA2 and STAGS for the three categories described in the introduction to this section: perfect shell, imperfect shell with imperfection amplitude set to zero, and imperfect shell with a nonzero imperfection amplitude. The smallest buckling load factors from the many STAGS models, 0.975, 0.964, 0.961, 0.978, indicate that the PANDA2 model for buckling of the perfect shell is slightly unconservative for buckling under Load Set 1. The buckling mode shape associated with the "best" (largest) STAGS model that yields a buckling load factor less than unity is shown in Figs. 20 - 22. This type of buckling is approximated best by the PANDA2 "patch" model with the domain that includes three bays in each of the two in-plane shell coordinate directions [9].

For the perfect shell it was time consuming to discover general buckling modes for model type "5" (the entire shell). They were embedded in a dense array of modes of the type displayed in Fig. 20. As shown especially in Figs. 23 and 24 the general modes are often "polluted" by local waviness. In the case of the imperfect shells with Zee stiffeners this "pollution" prevented the use of STAGS models of the type "5" for predicting collapse of the imperfect shells with general buckling modal imperfections.

In the case of the optimized imperfect Blade stiffened shell with imperfection amplitude Wimp = 0, the smallest few buckling eigenvalues are associated with simple ("pure") general modes of the type shown in Fig. 25. The first "semi"-general mode of the type displayed in Fig. 20 is associated with the ninth eigenvalue in this case. This fortunate characteristic holds for both load sets and makes it relatively easy to determine with STAGS the collapse load of the entire shell with a general buckling modal imperfection for each of the two load sets. Unfortunately, the optimized imperfect shells with Tee or Zee stiffeners behave differently.

There are two entries listed under P A N D A 2 R E S U L T S, one in the middle section of Table 16 and the other in the bottom section, that appear to conflict with the STAGS predictions. The values 1.046 and 1.034 that are listed under the heading "Stringer segment" are buckling load factors corresponding to Margin No. 7 in Table 9, “buckling margin stringer Iseg.3...”. In PANDA2 jargon "stringer Iseg.3" means buckling of the stringer web, or in cases involving Blade stiffeners, buckling of the stringer. With Blade stiffeners, PANDA2 assumes that the web root is simply supported (hinged) to the panel skin and the critical number of axial halfwaves in the buckling pattern of the stringer is equal to that found in the local buckling analysis of the panel skin. When the discretized skin-stringer panel module is used this critical number of axial halfwaves between rings is taken to be the one associated with the lowest buckling load factor corresponding to either Margin 1 or Margin 2 in Table 9. In this instance the critical number of axial halfwaves between rings is one for both the entry 1.046 (middle section of Table 16) and the entry 1.034 (bottom section). This PANDA2 model is usually a very conservative model of what happens in the actual very complex structure.

As seen from the STAGS predictions listed under the third category in Table 16 (bottom section), the load factors corresponding to collapse exceed unity for all the STAGS models. Unlike the PANDA2 model of buckling of the imperfect shells in which only ONE component of buckling modal imperfection is used, in the STAGS models TWO components of initial imperfection are introduced, one corresponding to a general buckling mode shape of the type shown in Fig. 25 and the other to a "panel" (inter-ring) mode shape of the type shown in Fig. 20. This difference in modeling between PANDA2 and STAGS seems justified because the optimum design of the imperfect Blade stiffened shell found by PANDA2 is associated with neighboring general buckling modes that have very different mode shapes, as discussed in connection with the data in Table 12 and Figs. 12 and 13. One of the mode shapes that is listed in the top section of Table 12 resembles the STAGS mode displayed in Fig. 25. The other, listed in the bottom section of Table 12, resembles the STAGS mode displayed in Fig. 20.

The maximum collapse load factor, 1.361, is obtained when only a general buckling component, Wimp(general), is introduced. (There is also a very, very small component Wimp(panel) = 0.0001 inch included to act as a trigger for incipient inter-ring bending in this case.) The collapse loads associated with the imperfection component Wimp (panel) = 0.01 in. are all fairly close. They are not strongly dependent on whether the general buckling modal component is present or whether it has 3 or 4 circumferential waves.

Figures 27 and 28 correspond to the Load Set 1 case with Wimp (general) = 0.025 inch with n = 4 circumferential waves and Wimp(panel) = 0.01 inch. The "collapse" load is near a load factor of 1.087. Figure 27 reveals that "collapse" occurs when the skin dimples inward very locally at certain discrete locations on the shell surface. A nearly identical pattern of local deformation repeats at 90-degree intervals around the

circumference, consistent with the $n = 4$ general buckling modal imperfection shape. Figure 28 shows the extreme fiber axial strain at one of the dimple peaks in the region where the nodal point density is the highest.

Note from Fig. 28 that the shell does not actually collapse at the load factor of 1.087, but carries additional load above this level. However, in the cases studied here we define failure as initial buckling, not total collapse. The shells are designed by PANDA2 with the local buckling load factor set equal to unity. Hence, local postbuckling is not allowed in the PANDA2 models investigated in this paper.

Figure 29 shows the collapse mode for the case when just Wimp(general) = 0.025 inch (n=3 circumferential waves) is included in the STAGS model. Collapse is indicated in Fig. 30 very near a load factor of 1.361 when the maximum hoop compression in the cylindrical skin at three circumferential locations and in the band where nodal point density is highest increases very steeply with load. The maximum hoop compression in the panel skin occurs where there is maximum inward circumferential bending. Since the rings are internal, overall inward circumferential bending of skin, stringers and rings as Wimp(general) is amplified by the increasing applied load subjects the cylindrical skin to increasing hoop compression. The rate at which the hoop compression develops grows approximately hyperbolically as the applied load approaches the collapse load. Nonlinear continuation fails as the primary nonlinear equilibrium path approaches a bifurcation near the load factor, 1.361. When the user-supplied maximum number of cuts in the load factor increment has been reached, STAGS computes eigenvalues corresponding to the current nonlinearly obtained equilibrium state and then terminates the run. The eigenvector corresponding to the smallest eigenvalue at the applied load factor of 1.361 is plotted in Fig. 31.

Figure 31 gives rise to a major question: why does bifurcation buckling from the primary equilibrium path occur in a region where the nodal point density is low? If the 480 finite element "converges from above" local buckling should have occurred somewhere in the band where the nodal point density is highest. A possible answer is that at the particular location where local buckling is predicted to occur perhaps there are higher destabilizing components of prebuckling compression than in the band with the highest nodal point density. In order to disprove this, another collapse case was run in which the three bands of higher nodal point density were moved from the midlength region of the shell, as shown in Fig. 29, and centered where local buckling occurs fairly near one end of the shell, as shown in Fig. 31. The same collapse load (to four significant figures!) and local buckling increment were found as before, with a similar local buckling mode but located this time elsewhere where the nodal point density is low (approximately in the region where the bands with high nodal point density used to be!)

Figures 32 and 33 reveal what is going on. Figure 32 shows the local distributions of prebuckling stress resultants Nx, Ny, Nxy in the panel skin at integration points in the finite elements where local buckling occurs as shown in Fig. 31 and at the load factor PA=1.361. The hoop component Ny is especially poorly estimated by the relatively crude local mesh. The values at the integration points are used in the bifurcation buckling analysis. The peak value of hoop compression, Ny = -125 lb/in, is six times greater than that plotted in Fig. 30 at the load factor 1.361. Figure 33 gives a comparison of the distributions of Ny from the crude and refined meshes at the same location (that shown at the local buckle displayed in Fig. 31) and at the same load. The unfortunate behavior demonstrated in Figs. 32 and 33 means that buckling and collapse predictions with use of the 480 finite element do not reliably "converge from above" with increasing nodal point density.

Results from STAGS for the Tee stiffened shells

Tables 17 and Fig. 34 contain the predictions. From these data one might conclude:

1. According to STAGS, with use of the best model (4,a,c,e,-,i,o) collapse occurs at a load factor of about 0.92 for Load Set 1 and 0.94 for Load Set 2.

2. It was not possible to find collapse with models of the type "5" because the general buckling modes could not be gleaned from dense thickets of local modes involving either relatively short axial wavelength rolling of the stringers or inter-ring buckling of the types “2” or “4.” Models of type “5” with cruder meshes that can be used to obtain general buckling modes cannot have both sets of stiffeners treated as shell branches combined with a locally fine enough mesh to capture local dimpling of the skin in the collapse mode, as shown for the Blade stiffened shell in Fig. 27.

3. For the optimized perfect shell the STAGS models of type "2" predict skin buckling to occur at a load factor about 35 per cent higher than that predicted with PANDA2. As with the Blade stiffened shell, the difference is due to the presence of the

stiffeners in the STAGS model. In this respect PANDA2 is perhaps too conservative.

4. For Load Set 1 the inclusion of fasteners raises the buckling load factor associated with bifurcation buckling of type "2,3" much more than it influences the collapse load factor. Whether or not fasteners are included has little effect on load factors associated with general buckling or the load factors associated with buckling under Load Set 2.

5. As might be expected, the prediction of general bifurcation buckling is not strongly affected by the details of the model, as long as it is of type "5". Note, however, that this would probably not be true of collapse because "collapse", as defined in this paper, is associated with the development of relatively tiny dimples in the panel skin, as shown in Fig. 27 for the Blade stiffened shell. In order to capture the growth of these dimples one requires a locally fine mesh with at least the adjacent stiffeners treated as branched shells. Time did not permit the development of STAGS models in which different models of the stiffeners are used in different regions of the shell.

6. There is not a dramatic difference in predictions from models of the type "3" vs models of the type "4". It is probably best to limit the overall size of the STAGS model (e.g. choose Model type "3" rather than "4") if this is necessary in order to be able to retain the detailed branched shell representation of the stiffeners.

7. It is best to prevent sidesway of the stiffeners at the edges of the shell.

8. It is best to prevent in-plane warping of the panel skin along the two straight edges.

There is one entry listed under P A N D A 2 R E S U L T S in the top, middle and bottom sections of Table 17 that may seem at odds with the STAGS predictions: the value 0.997 for buckling of a stringer segment under Load Set 1. This buckling load factor in the case of the Tee stiffened shell corresponds to Margin No. 10 in Table 9, "stringer Iseg 4 as beam on foundation". In PANDA2 jargon "stringer Iseg 4" is the outstanding flange. This flange is supported by the stringer web. The outstanding flange can buckle in such a direction as to compress and extend the web in a trigonometric variation along the axis of the stringer. In this mode the primary buckling modal direction is normal to the surface of the outstanding flange. Buckling of this type is usually associated with a very high load factor because there is a lot of membrane strain energy required for the web to deform in its plane. In PANDA2 a buckling model is set up [10] that represents the web as a Winkler foundation. A factor of safety of three is more-or-less arbitrarily assigned by PANDA2 to this mode of failure. Hence, the "beam on foundation" model is probably very conservative, both because of the rather large factor of safety provided internally by PANDA2 and because the in-plane shearing of the web in this unusual buckling mode is ignored in the PANDA2 Winkler model. The conservative model was used in PANDA2 in order to stay far away from designs in which it is possible for the outstanding flange to tear away from the web as axial compression is applied and a possibly initially wavy flange bends further under increasing compression, subjecting the web to in-plane normal and shear stresses, and severe stress concentration where the web joins the outstanding flange.

Figure 34 shows load deflection curves for the various STAGS models for the panels and shells collapsing under Load Set 1. The best model of all those depicted, 4,a,c,e,-,i,o,u, corresponds to the second-to-last item in the legend.

Results from STAGS for the Zee stiffened shells

Tables 18 and Figs. 35 - 39 contain the predictions. From these data one might conclude:

1. As with the Tee stiffened shells, the STAGS model type "2" predicts buckling of the panel skin to occur at a load factor considerably higher than that predicted with the PANDA2 model. The difference is again due to the presence of the stiffeners in the STAGS model of local skin buckling which in these cases resist rotation of the skin at the edges of the domain included in the STAGS model.

2. The effect of fasteners is significantly to strengthen the structure, both with regard to bifurcation buckling and collapse. The effect of the fasteners on the collapse load is greater for the Zee stiffened shell than for the Tee stiffened shell because the thickness of the stringer faying flange for the Zee stiffened optimized imperfect shell is greater than that for the Tee stiffened shell and the height of the stringer web is less (Table 8). Figure 35 shows nonlinear load-deflection curves for type "3" models with and without fasteners.

3. The load factor for general instability is significantly affected by the modeling of the rings in STAGS models of type "5". If the rings are

smeared or treated as discrete beams (210 elements) a load factor of about 3.0 is computed for the optimized imperfect shell with Wimp = 0. With the rings modeled as shell branches a load factor of about 2.1 is computed. PANDA2 models with Zee stiffeners show the same effect [10]. The pronounced influence of careful ring modeling is due to the fact that with Zee stiffeners, which are not bilaterally symmetric, the cross sections of the stiffeners deform significantly in the general buckling mode. The cross sections of the Tee stiffeners do not exhibit this behavior.

4. Although general buckling modes were found with STAGS model type "5" for both Load Set 1 and Load Set 2, it was not possible to obtain converged results for collapse with use of the "5" model because there is too much "pollution" of the general buckling mode with local waviness for "5" models in which there is sufficient local midlength refinement of the nodal mesh to capture local dimpling of the skin as shown in Fig. 27, for example. Figures 36 - 39 demonstrate the attempts to compute collapse loads with use of a type "5" STAGS model with Load Set 2. Figure 36 shows the $n = 3$ general buckling mode with use of a type "5" model in which each single 4.0 x 1.885 in. bay in the central region of the shell has 6 x 2 480 finite elements. The search for this mode is somewhat tedious because it is hidden among a rather dense array of inter-ring modes of the type shown in Fig. 37, which represents the fundamental buckling mode for this STAGS model. Several nonlinear load deflection curves are displayed in Fig. 38 in which various combinations of general and inter-ring buckling modal imperfections are used. All of the curves are felt to be unacceptably unconservative because the 6 x 2 480 finite element grid in each bay in the central region of the shell is not refined enough to capture local buckling and collapse of the panel skin, as shown in Fig. 27. Figure 39 shows a more refined model in which in a central three-ring-bay-region each 4.0 x 1.885 inch panel skin bay has 12 x 3 480 finite elements. This STAGS type "5" model has almost 356000 degrees of freedom. Unfortunately, the "general" buckling mode shown in Fig. 40 cannot be used as an imperfection shape because there is too much "pollution" by localbuckling.

Summary of collapse behavior

Figure 40 shows load deflection curves for the optimized imperfect shells with Blade, Tee, and Zee stiffeners for both Load Set 1 and Load Set 2. Results from the best possible models for each case are plotted. The PANDA2 predictions of failure of the optimized imperfect shell with Tee stiffeners is about eight per cent unconservative and for the optimized imperfect shell with Zee stiffeners is about two per cent unconservative, according to the STAGS predictions. The two curves for the Blade stiffened shell that display the largest maximum normal displacement w include the overall bending in an $n = 4$ general buckling mode of the type shown in Fig. 25 (but with $n = 4$ rather than $n = 3$). This overall mode is not present for the other curves, which are derived from STAGS models type "4" rather than type "5".

The weakest link

It is emphasized that the quality of the comparison between PANDA2 and STAGS predictions for the failure of the optimized imperfect shells is diminished by the fact that different initial imperfections are used in the PANDA2 and STAGS models. In the PANDA2 models a general buckling modal imperfection with amplitude 0.025 inch was used. A question arises, "What is the general buckling mode?" During optimization cycles in SUPEROPT runs with PANDA2 the shape of the general buckling modal imperfection often changes radically from design iteration to iteration, as explained in the discussion associated with Table 12 and Figs. 12 and 13. For the Blade stiffened shell the final optimum design has a general buckling modal imperfection shape that resembles that shown in Fig. 25. However, as demonstrated in Table 12 and in Fig. 14, the optimum design is very like neighboring designs for which the general buckling mode is more like that displayed in Fig. 20 than that in Fig. 14. Use of the simple $n = 3$ or $n = 4$ overall general buckling mode with the long axial and circumferential wavelengths in STAGS models is much more benign than use the much shorter wavelength imperfection. (Compare the collapse load factor 1.361 and collapse mode shown in Fig. 29 for the case Wimp(general) = 0.025 inch, Wimp(panel) = 0.0001 inch with the collapse load factor 1.087 and collapse mode shown in Fig. 27 for the case Wimp(general) = 0.025 inch, Wimp(panel) = 0.01 inch, the fourth from last and third from last entries in Table 16.) The lurking proximity of the shorter-wavelength general buckling modes during PANDA2 optimizations influences the evolution of the optimum designs. Therefore, it was decided to include a mixture of the two types of buckling modes in the STAGS models of type "5". For the Tee and Zee stiffened shells the type "5" model could not be used to obtain reliable collapse loads, as explained previously. Therefore, only buckling modal imperfection shapes that resemble the relatively short wavelength modes in Figs. 18, 19a, and 20, for exa m-

ples, could be used in these cases. It was more-or-less arbitrarily decided to assign a magnitude of 0.01 inch to the initial amplitude of modes of this less benign type. It is unlikely that in practice such short-wavelength imperfections with larger amplitudes than 0.01 inch would survive reasonably careful inspections of manufactured stiffened shells of the rather small size investigated here.

CONCLUSIONS

Activity

A new PANDA2 processor called STAGSUNIT was developed. This computer program uses the PANDA2 database and some simple input from the user to generate input files for STAGS for optimized composite cylindrical shells stiffened by stringers and/or rings with Blades, Tee, Jay or Zee cross sections. The panels or complete (360 deg.) shells can be loaded by combined axial compression, hoop compression, in-plane shear and normal pressure. Particular care was taken during the development of STAGSUNIT to establish edge conditions that permit the use of subdomains of a large shell structure without introducing local stress constraints near the boundaries of the subdomain. A variety of models of the stiffeners and stiffener segments is permitted. The stiffeners can be connected directly to the cylindrical skin or they can be linked to the skin with fasteners.

Comparisons were made for buckling and collapse of optimized perfect and optimized imperfect angle-ply cylindrical shells stiffened by Blades or Tees or Zees made of orthotropic material. A variety of STAGS models, all generated via STAGSUNIT, were generated and processed for each geometry. In every case there were both stringers and rings.

Conclusions

1. For stiffened shells PANDA2 predictions for local buckling of the panel skin are quite conservative. The difference between PANDA2 and STAGS predictions for skin buckling are caused by the presence of stiffeners in the STAGS models. For the optimum designs in the cases studied here the stiffeners tend to resist rolling as the skin buckles locally.

2. The failure loads predicted by PANDA2 and the collapse loads predicted by STAGS for the optimized imperfect shells agree fairly well, certainly well enough to justify the use of PANDA2 for preliminary design.

3. Occasionally both the 410 and the 480 finite elements in the STAGS element library produce unreliable predictions. Sometimes the 410 element shows buckling where the finite element mesh is sparse and no buckling where the mesh is dense, even though the prebuckled state is uniform. In regions of relatively low nodal point density the 480 element produces inaccurate distributions of prebuckling hoop resultant at the integration points, values that are used in the buckling analysis and therefore affect buckling load factors. Unfortunately the maximum compressive hoop resultant at the integration points of the finite element may be greatly overestimated where the nodal point density is low, possibly leading to predictions that do not converge from above with increasing nodal point density.

4. During optimization cycles involving imperfect shells, the PANDA2 margins sometimes oscillate wildly from cycle to cycle, making it difficult to find a global optimum design. These oscillations are caused by alternating dramatic changes in the predicted general buckling mode shape of the imperfect shell. This phenomenon has an especially strong influence on the prediction of local buckling of the panel skin because the prebuckled state of the panel skin is strongly affected by prebuckling bending of the stiffened imperfect shell as the initial buckling modal imperfection is amplified under loading. The effective circumferential radius of curvature of the skin is strongly influenced by the number of circumferential waves in the general buckling modal imperfection.

5. In STAGS models involving the entire shell, appropriate general buckling modes of the optimized shells could often not be gleaned from dense thickets of local modes with lower or similar eigenvalues. Sometimes the general modes could be found but they would be too “polluted” by local waves to designate as appropriate general buckling modal imperfections.

Suggestions for more work

1. A 280 beam element should be introduced into STAGS to work with the 480 shell element.

2. The STAGS eigenvalue extraction strategy should be modified to permit more eigenvalues to be determined in a single run.

3. During the development of STAGSUNIT a particularly tricky area was that involving the elimination of "drilling" freedoms whenever the 480 finite element is used in the STAGS model. It would be beneficial for users who set up STAGS models without a program like STAGSUNIT to have STAGS deal internally with the problem of "drilling" freedoms. The same might be written with regard to the introduction of fasteners. It would be beneficial to have STAGS automatically recognize gaps between shell unit junctions and to prompt the user for fastener properties only, not make the user count nodal points, etc. As presently set up it is too easy for the user to make errors in input that do not show up in plots or as error messages in the STAGS output.

4. The STAGSUNIT program should be expanded to permit different modeling in different regions of a stiffened cylindrical shell. For example, it would be useful to be able generate STAGS models in which one or both sets of stiffeners are smeared over part of the shell and modeled as shell units over other parts.

5. Now that the program STAGSUNIT has been written, it might be possible automatically and cyclicly to set up a number of STAGS models that can be used together in an optimization context. For example, small models of the types "1" and "2" (Table 13) could be used to capture local skin buckling; larger models of the type "3" could be used to capture inter-ring buckling; and the largest models of type "5" with crude meshes and smeared stiffeners could be used to capture general buckling. If the STAGS processors (S1 and S2) could be transformed into subroutines, it might be feasible to introduce STAGS into a system, such as GENOPT [31]. This was done with BOSOR4, as reported in [32].

ACKNOWLEDGMENTS

David Bushnell very much appreciates the help of Dr. Frank Weiler, who set up a computer in Bushnell's office where Bushnell could easily view STAGS results. Dr Weiler also responded promptly if there were any problems running very large STAGS cases (356000 degrees of freedom, the largest case run here, works!). Bushnell is also grateful to Dr. William Loden, who helped Bushnell work his way through the STAGS input documentation dealing with rigid links and fasteners and who created Figs. 5 and 6 on the computer.

REFERENCES

[1] Bushnell, D., "PANDA2 - program for minimum weight design of stiffened, composite, locally buckled panels", Computers and Structures, Vol. 25, No. 4, 469- 605 (1987).

[2] Bushnell, D., "Theoretical basis of the PANDA computer program for preliminary design of stiffened panels under combined in-plane loads", Computers and Structures, Vol. 27, No. 4, 541-563 (1987).

[3] Bushnell, D., "Optimization of composite, stiffened, imperfect panels under combined loads for service in the postbuckling regime", Computer Methods in Applied Mechanics and Engineering, Vol. 103, 43-114 (1993).

[4] Bushnell, D. and Bushnell, W. D., "Minimum-weight design of a stiffened panel via PANDA2 and evaluation of the optimized panel via STAGS", Computers and Structures, Vol. 50, 569-602 (1994).

[5] Bushnell, D. and Bushnell, W. D., "Approximate method for the optimum design of ring and stringer stiffened cylindrical panels and shells with local, inter-ring, and general buckling modal imperfections", Computers and Structures, Vol. 59, No. 3, 489-527 (1996).

[6] Bushnell, D., "Recent enhancements to PANDA2", AIAA Paper 96-1337-CP, 37th AIAA Structures, Structural Dynamics and Materials Conference, April, 1996. See also, "Global optimum design of externally pressurized isogrid stiffened cylindrical shells with added T-rings", Int. J. of Non-linear Mech., Vol.37, Nos. 4 & 5 (2002).

[7] Bushnell, D., "Optimum design via PANDA2 of composite sandwich panels with honeycomb or foam cores", AIAA Paper 97-1142, Proceedings of the AIAA 38th Structures, Structural Dynamics, and Materials Conference, 2163–2202 April 1997.

[8] Bushnell, D., "Optimization of panels with riveted Z-shaped stiffeners via PANDA2, in Advances in the Mechanics of Plates and Shells", Durban, D, Givoli, D., and Simmonds, J.G., Eds, Kluwer Academic Publishers, 79-102, 2001. See also, Proc. 39th AIAA Structures, Materials and Dynamics meeting, 2357-2388, AIAA. 1998.

[9] Bushnell, D., Jiang, H. and Knight, N.F. Jr. "Additional buckling solutions in PANDA2", AIAA Paper 99-1233, Proceedings of the AIAA 40th Structures, Structural Dynamics, and Materials Conference, 302-345, April 1999.

[10] Bushnell, D., unpublished file called ...panda2/doc/panda2.news which contains a log of all PANDA2 changes since 1987.

[11] Almroth, B. O. and Brogan, F. A., "The STAGS computer code", NASA CR-2950, NASA Langley Research Center, Hampton, VA, 1978.

[12] Rankin, C. C., Stehlin, P., and Brogan, F. A., "Enhancements to the STAGS computer code", NASA CR-4000, NASA Langley Research center, Hampton, VA, 1986.

[13] Riks, E., Rankin C. C., Brogan F. A., "On the solution of mode jumping phenomena in thin walled shell structures", First ASCE/ASM/SES Mechanics Conference, Charlottesville, VA, June 6-9, 1993, in: Computer Methods in Applied Mechanics and Engineering, Vol.136, pp. 59–92 (1996).

[14] Viswanathan, A. V. and Tamekuni, M., "Elastic buckling analysis for composite stiffened panels and other structures subjected to biaxial inplane loads", NASA CR- 2216, September 1973.

[15] Dickson, J. N., Biggers, S. B. and Wang, J. T. S., "Preliminary design procedure for composite panels with open-section stiffeners loaded in the post-buckling range," in: Advances in Composite Materials, A. R. Bunsell, et al,editors, Pergamon Press Ltd., Oxford, England, 1980, 812-825. Also see, J. N. Dickson and S. B. Biggers, "POSTOP: Postbuckled open- stiffened optimum panels, theory and capability", NASA Langley Research Center, Hampton, Va., NASA Contractor Report from NASA Contract NAS1 - 15949, May 1982.

[16] Butler, R. and Williams, F. W., "Optimum design features of VICONOPT, an exact buckling program for prismatic assemblies of anisotropic plates," AIAA Paper 90-1068- CP, Proceedings 31st AIAA/ASME Structures, Structural Dynamics, and Materials Meeting, 1289-1299. Also see Williams, F. W., Kennedy, D., Anderson, M.S., "Analysis features of VICONOPT, an exact buckling and vibration program for prismatic assemblies of anisotropic plates,", AIAA Paper 90-0970-CP, Proceedings 31st AIAA/ASME Structures, Structural Dynamics, and Materials Meeting, 920-929. Also see Kennedy, D., Powell, S. and Williams, F., "Local postbuckling analysis for perfect and imperfect longitudinally compressed plates and panels", AIAA-98-1770, 39th AIAA/ASME Structures, Structural Dynamics, and Materials Meeting, 1998.

[17] Anderson, M. S. and Stroud, W. J., "General panel sizing computer code and its application to composite structural panels," AIAA Journal, 17, 892-897 (1979). Also see W. J. Stroud and M. S. Anderson, "PASCO: Structural panel analysis and sizing code, capability and analytical foundations," NASA TM-80181, NASA Langley Research Center, Hampton, Va., 1981. Also see W. J. Stroud, W. H. Greene and M. S. Anderson, "Buckling loads of stiffened panels subjected to combined longitudinal compression and shear: Results obtained with PASCO, EAL, and STAGS computer programs," NASA TP 2215, Nasa Langley Research Center, Hampton, Va., January 1984.

[18] Bushnell, D., "BOSOR4: Program for stress, buckling, and vibration of complex shells of revolution," Structural Mechanics Software Series - Vol. 1, (N. Perrone and W. Pilkey, editors), University Press of Virginia, Charlottesville, 11-131 (1977). See also Computers and Structures, Vol. 4, 399-435 (1974); AIAA J, Vol. 9, No. 10, 2004-2013 (1971); Structural Analysis Systems, Vol. 2, A. Niku-Lari, editor, Pergamon Press, Oxford, 25-54 (1986): and Computers and Structures, 18, (3), 471-536 (1984).

[19] Vanderplaats, G. N. and Sugimoto, H., "A general-purpose optimization program for engineering design", Computers and Structures, 24, 13-21 (1986).

[20] Arbocz, J., "The effect of initial imperfections on shell stability - An updated review", Delft University Faculty of Aerospace Engineering Report LR-695, September 1992.

[21] Arbocz, J. and Hol, J. M. A. M., "On the reliability of buckling load predictions", AIAA Paper 94-1371, Proc. 35th AIAA Structures, Structural Dynamics, and Materials Conference, Hilton Head SC, 514-527 (1993).

[22] Arbocz, J. and Hol, J., "Shell stability analysis in a computer aided engineering (CAE) environment", AIAA Paper 93-133, Proc. 34th AIAA Structures, Structural Dynamics, and Materials

Conference, La Jolla, CA, 300-314 (1993).

[23] Bauld, N. R. Jr. and Khot, N. S., "A numerical and experimental investigation of the buckling behavior of composite panels", Computers and Structures, 15 393-403 (1982).

[24] Khot, N. S. and Bauld, N. R. Jr., "Further comparison of the numerical and experimental buckling behaviors of composite panels," Computers and Structures, 17, 61-68 (1983).

[25] Koiter, W. T., "Het Schuifplooiveld by Grote Overshrijdingen van de Knikspanning," Nationaal Luchtvaart Laboratorium, The Netherlands, Report X295, November 1946 (in Dutch).

[26] Stanley, G. "The Computational Structural Mechanics Testbed Structural Element Processor ES1: Basic SRI and ANS Shell Elements," NASA CR-4357, 1991.

[27] Rankin, C. and Brogan, F. "The Computational Structural Mechanics Testbed Structural Element Processor ES5: STAGS Shell Element," NASA CR-4358, 1991.

[28] Baruch, M. and Singer, J. "Effect of eccentricity of stiffeners on general instability of stiffened cylindrical shells under hydrostatic pressure", J. Mech. Engrg Sci., Vol. 5, 23-27 (1963).

[29] Koiter, W. T., "The effect of axisymmetric imperfections on the buckling of cylindrical shells under axial compression". Kononkl. Ned. Akad. Wetenschap. Proc. B66, 265-279 (1963).

[30] Sanders, J. L. Jr., "Nonlinear theories for thin shells", Quarterly Applied Math, Vol. 21, 21-36, 1963. Also see, "An improved first-approximation theory for thin shells", NASA TR R-24, Langley Research Center, 1959.

[31] Bushnell, D., "GENOPT - a program that writes user-friendly optimization code", Int. J. Solids, Struct., Vol. 26, No. 9/10, 1173-1210 (1990).

[32] Bushnell, D., "Automated design of shells of revolution with application to ring-stiffened cylindrical shells with wavy walls", AIAA Paper No. 2000-1663, 41st AIAA Structures, Structural Dynamics and Materials Conference, April 2000.

Table 1 Input data for the new PANDA2 processor called STAGSUNIT

```
n          $ Do you want a tutorial session and tutorial output?
  1        $ Choose type of STAGS analysis (1,3,4,5,6),INDIC
  0        $ Restart from ISTARTth load step (0=1st nonlinear soln), ISTART
  3        $ Local buckling load factor from PANDA2, EIGLOC
y          $ Are the dimensions in this case in inches?
  0        $ Lowest vibration frequency (cps) from STAGS INDIC=5 run, CPS
  0        $ Percent damping to be used in STAGS transient (INDIC=6) run.
 14        $ X-direction length of the STAGS model of the panel: XSTAGS
  8        $ Panel length in the plane of the screen, L2
y          $ Is the nodal point spacing uniform along the stringer axis?
 41        $ Number of nodes in the X-direction: NODEX
-700       $ Resultant (e.g. lb/in) normal to the plane of screen, Nx
  0        $ Resultant (e.g. lb/in) in the plane of the screen,    Ny
 40        $ In-plane shear in load set A,                         Nxy
  0        $ Uniform applied pressure [positive upward. See H(elp)], p
  0        $ Resultant (e.g. lb/in) normal to the plane of screen, Nx0
  0        $ Resultant (e.g. lb/in) in the plane of the screen,    Ny0
  0        $ Uniform applied pressure [positive upward. See H(elp)], po
  1        $ Starting load factor for Load System A, STLD(1)
  0        $ Load factor increment for Load System A, STEP(1)
  1        $ Maximum load factor for Load System A, FACM(1)
  0        $ Starting load factor for Load System B, STLD(2)
  0        $ Load factor increment for Load System B, STEP(2)
  0        $ Maximum load factor for Load System B, FACM(2)
  1        $ How many eigenvalues do you want? NEIGS
480        $ Choose element type (410 or 411 or 480) for panel skin
n          $ Have you obtained buckling modes from STAGS for this case?
 20        $ Number of stringers in STAGS model of 360-deg. cylinder
  3        $ Number of rings in STAGS model of 360-deg. cylinder
y          $ Are there rings at the ends of the cylindrical shell?
  4        $ Number of finite elements between adjacent stringers
 10        $ Number of finite elements between adjacent rings
  3        $ Stringer model: 1 or 2 or 3 or 4 or 5(Type H(elp))
  3        $ Ring model: 1 or 2 or 3 or 4 or 5 (Type H(elp))
  0        $ Reference surface of cyl: 1=outer, 0=middle, -1=inner
y          $ Do you want to use fasteners (they are like rigid links)?
n          $ Are the stringers to be "smeared out"?
n          $ Are the rings to be "smeared out"?
  5        $ Number of nodes over height of stiffener webs, NODWEB
n          $ Do you want to use the "least-squares" model for torque?
n          $ Is stiffener sidesway permitted at the panel edges?
  1        $ Edges normal to screen (0) in-plane deformable; (1) rigid
```

Table 2 The first part of the *.inp file produced by STAGSUNIT

```
 isaact STAGS INPUT FOR STIFFENED CYL.(STAGSUNIT=SHELL UNITS)
C
C Begin B-1 input data...
 0,  $ IGRAV =0 means g = 386.4 inches per sec.**2; else B-4
 0,  $ ICHECK=0 means normal execution
 0,  $ ILIST =0 means normal batch-oriented output
 0,  $ INCBC=0:buck. bcs same as prebuc; 1: different.
 0,  $ NRUNIT=0 means plot entire model.
 3,  $ NROTS=3 means plot model with 3 rotations, as on B-1b.
 1   $ KDEV=1 means use PostScript file format for plot.END B-1
 1,  $ IROT=1 means rotation about global X-axis.BEGIN B-1b
 -35.84  $ ROT=0 means rotate 0 deg. about global X-axis.END B-1b
 2,  $ IROT=2 means rotation about global Y-axis.BEGIN B-1b
 -13.14  $ ROT=80 means rotate 80 deg. about global Y-axis.END B-1b
 3,  $ IROT=3 means rotation about global Z-axis.BEGIN B-1b
 35.63  $ ROT=0 means rotate 0 deg. about global Z-axis.END B-1b
C
C Begin B-2 input data...
  19, $ NUNITS=number of shell units.            BEGIN B-2 rec.
   6, $ NUNITE=number of fasteners = finite element units
   0, $ NSTFS = number of shell units with discrete stiffeners
   0, $ NINTS means number of connections between shell units
  43, $ NPATS=number of records for partial nodal compatibility
 -174, $ NCONST= number of Lagrange constraint conditions
 0, $ NIMPFS=number of bucklng modal imperfections.
 0, $ INERT = 0 means no inertial load records
 0  $ NINSR = 0 means no crack tip element sets. END B-2 rec.
C
C Begin B-3 input data...
16, $ NTAM = number of entries in material tabl.BEGIN B-3 rec.
12, $ NTAB = number of beam cross section entries
13, $ NTAW = number of entries in shell wall table.
 0, $ NTAP = 0 means user parameters not included.
 1  $ NTAMT = 1 means one spring element table.END B-3 rec.
C
C Begin B-4, B-5 input data, if any...
C
C Begin F-1 input data (discretization)...
  41  17, $ F-1 NROWS( 1),  NCOLS( 1) unit 1 = cyl. shell
  41   5, $ f-1 fayflange NROWS(  2), NCOLS(  2) Unit   2 stringer no.  1
  41   5, $ f-1 strng.web NROWS(  3), NCOLS(  3) Unit   3 stringer no.  1
  41   5, $ f-1 outflange NROWS(  4), NCOLS(  4) Unit   4 stringer no.  1
  41   5, $ f-1 fayflange NROWS(  5), NCOLS(  5) Unit   5 stringer no.  2
  41   5, $ f-1 strng.web NROWS(  6), NCOLS(  6) Unit   6 stringer no.  2
  41   5, $ f-1 outflange NROWS(  7), NCOLS(  7) Unit   7 stringer no.  2
  41   5, $ f-1 fayflange NROWS(  8), NCOLS(  8) Unit   8 stringer no.  3
  41   5, $ f-1 strng.web NROWS(  9), NCOLS(  9) Unit   9 stringer no.  3
  41   5, $ f-1 outflange NROWS( 10), NCOLS( 10) Unit  10 stringer no.  3
   5  17, $ f-1 fayflange NROWS( 11), NCOLS( 11) Unit  11   ring   no.  1
   5  17, $ f-1  ring web NROWS( 12), NCOLS( 12) Unit  12   ring   no.  1
   5  17, $ f-1 outflange NROWS( 13), NCOLS( 13) Unit  13   ring   no.  1
   5  17, $ f-1 fayflange NROWS( 14), NCOLS( 14) Unit  14   ring   no.  2
   5  17, $ f-1  ring web NROWS( 15), NCOLS( 15) Unit  15   ring   no.  2
   5  17, $ f-1 outflange NROWS( 16), NCOLS( 16) Unit  16   ring   no.  2
   5  17, $ f-1 fayflange NROWS( 17), NCOLS( 17) Unit  17   ring   no.  3
   5  17, $ f-1  ring web NROWS( 18), NCOLS( 18) Unit  18   ring   no.  3
   5  17  $ f-1 outflange NROWS( 19), NCOLS( 19) Unit  19   ring   no.  3
```

Table 3 The *.bin file produced by STAGSUNIT

```
 isaact STAGS INPUT FOR STIFFENED CYL.(STAGSUNIT=SHELL UNITS)
 1, $ INDIC=1 is bifur.buckling; INDIC=3 is nonlinear BEGIN B-1
 1, $ IPOST=1 means save displacements every IPOSTth step
 0, $ ILIST =0 means normal batch-oriented output
 0, $ ICOR  =0 means projection in; 1 means not in.
 1, $ IMPTHE=index for imperfection theory.
 0, $ ICHIST=index for crack archive option
 0, $ IFLU  =0 means no fluid interaction.
 -1 $ ISOLVR= 0 means original solver; -1 new solver.END B-1 rec
 1.000E+00, $ STLD(1) = starting load factor, System A. BEGIN C-1 rec.
 0.000E+00, $ STEP(1) = load factor increment, System A
 1.000E+00, $ FACM(1) = maximum load factor, System A
 0.000E+00, $ STLD(2) = starting load factor, System B
 0.000E+00, $ STEP(2) = load factor increment, System B
 0.000E+00, $ FACM(2) = maximum load factor, System B
 0      $ ITEMP =0 means no thermal loads. END C-1 rec.
 10000, $ NSEC= number of CPU seconds before run termination
 0.,    $ DELEV is eigenvalue error tolerance (0=.00001)
 0      $ IPRINT=0 means print modes, iteration data, END D-2 rec.
 1,     $ NEIGS= number of eigenvalues sought.  BEGIN D-3 rec.
 2.100E+00, $ SHIFT=initial eigenvalue shift
 0.000E+00, $ EIGA =lower bound of eigenvalue range
 0.000E+00  $ EIGB =upper bound of eigenvalue range.      END D-3 rec.
```

Table 4 Headings in the *.inp file for the case shown in Fig.1

```
 isaact STAGS INPUT FOR STIFFENED CYL.(STAGSUNIT=SHELL UNITS)
C Begin B-1 input data...
C Begin B-2 input data...
C Begin B-3 input data...
C Begin B-4, B-5 input data, if any...
C Begin F-1 input data (discretization)...
C Begin partial compatability (g-2) records.
C Partial compatability (g-2) records for the cylindrical shell
C Partial compatability (g-2) records for stringer  1
C Partial compatability (g-2) records for stringer  2
C Partial compatability (g-2) records for stringer  3
C Partial compatability (g-2) records for the rings.
C Partial compatability (g-2) records for ring  1
C Partial compatability (g-2) records for ring  2
C Partial compatability (g-2) records for ring  3
C lagrange constraints for stringer sidesway
C lagrange constraints for ring sidesway
C Lagrange constraints for linear variation of u at y=0
C Lagrange constraints for linear variation of u at y=YSTAGS
C Lagrange constraints for linear variation of v at y=0
C Lagrange constraints for linear variation of v at y=YSTAGS
C Fasteners for stringers...
C Fasteners for rings...
C Material in one or more of shell unit walls NOT at an edge
C Material in one or more of shell unit walls NOT at an edge
C Matl in one or more shell unit walls that form edge stiffners
C Matl in one or more shell unit walls that form edge stiffners
C Not edge; stringer; fayflnge (equivalent matl for beam)
C Not edge; stringer;   web    (equivalent matl for beam)
C Not edge; stringer; outflnge (equivalent matl for beam)
C Not edge;   ring  ; fayflnge (equivalent matl for beam)
C Not edge;   ring  ;   web    (equivalent matl for beam)
C Not edge;   ring  ; outflnge (equivalent matl for beam)
C  At edge; stringer; fayflnge (equivalent matl for beam)
C  At edge; stringer;   web    (equivalent matl for beam)
C  At edge; stringer; outflnge (equivalent matl for beam)
C  At edge;   ring  ; fayflnge (equivalent matl for beam)
C  At edge;   ring  ;   web    (equivalent matl for beam)
C  At edge;   ring  ; outflnge (equivalent matl for beam)
C  Fastener property table...
C Not edge; stringer; fayflnge (beam cross section props)
C Not edge; stringer;   web    (beam cross section props)
C Not edge; stringer; outflnge (beam cross section props)
```

Table 4 (continued)

```
C Not edge;   ring  ; fayflnge (beam cross section props)
C Not edge;   ring  ;   web    (beam cross section props)
C Not edge;   ring  ; outflnge (beam cross section props)
C  At edge; stringer; fayflnge (beam cross section props)
C  At edge; stringer;   web    (beam cross section props)
C  At edge; stringer; outflnge (beam cross section props)
C  At edge;   ring  ; fayflnge (beam cross section props)
C  At edge;   ring  ;   web    (beam cross section props)
C  At edge;   ring  ; outflnge (beam cross section props)
C Not edge; cyl.skin;   skin   (shell unit wall props   )
C Not edge; stringer; fayflnge (shell unit wall props   )
C Not edge; stringer;   web    (shell unit wall props   )
C Not edge; stringer; outflnge (shell unit wall props   )
C Not edge;   ring  ; fayflnge (shell unit wall props   )
C Not edge;   ring  ;   web    (shell unit wall props   )
C Not edge;   ring  ; outflnge (shell unit wall props   )
C  At edge; stringer; fayflnge (shell unit wall props   )
C  At edge; stringer;   web    (shell unit wall props   )
C  At edge; stringer; outflnge (shell unit wall props   )
C  At edge;   ring  ; fayflnge (shell unit wall props   )
C  At edge;   ring  ;   web    (shell unit wall props   )
C  At edge;   ring  ; outflnge (shell unit wall props   )
C Begin unit 1: cylindrical shell
C Input for boundary conditions...
C Loads applied to panel skin...
C Drilling freedoms suppressed in cyl. skn
C  Bay no.  1; drilling degrees of freedom suppressed
C  Bay no.  2; drilling degrees of freedom suppressed
C Output control...
C Begin unit  2: faying flange of stringer no.  1
C Drilling freedoms suppressed in stringer faying flange
C Begin unit  3: web of stringer no.  1
C Drilling freedoms suppressed in stringer web
C Begin unit  4: outstanding flange of stringer no.  1
C Drilling freedoms suppressed in stringer outstanding flange
C Begin unit  5: faying flange of stringer no.  2
C Drilling freedoms suppressed in stringer faying flange
C Begin unit  6: web of stringer no.  2
C Drilling freedoms suppressed in stringer web
C Begin unit  7: outstanding flange of stringer no.  2
C Drilling freedoms suppressed in stringer outstanding flange
C Begin unit  8: faying flange of stringer no.  3
C Drilling freedoms suppressed in stringer faying flange
C Begin unit  9: web of stringer no.  3
C Drilling freedoms suppressed in stringer web
C Begin unit 10: outstanding flange of stringer no.  3
C Drilling freedoms suppressed in stringer outstanding flange
C Begin unit 11: faying flange of ring no.  1
C Drilling freedoms suppressed in ring faying flange
C Begin unit 12: web of ring no.  1
C Drilling freedoms suppressed in ring web
C Begin unit 13: outstanding flange of ring no.  1
C Drilling freedoms suppressed in ring outstanding flange
C Begin unit 14: faying flange of ring no.  2
C Drilling freedoms suppressed in ring faying flange
C Begin unit 15: web of ring no.  2
C Drilling freedoms suppressed in ring web
C Begin unit 16: outstanding flange of ring no.  2
C Drilling freedoms suppressed in ring outstanding flange
C Begin unit 17: faying flange of ring no.  3
C Drilling freedoms suppressed in ring faying flange
```

Table 4 (Continued)

```
C Begin unit 18: web of ring no.  3
C Drilling freedoms suppressed in ring web
C Begin unit 19: outstanding flange of ring no.  3
C Drilling freedoms suppressed in ring outstanding flange
C  fastener for stringer number  1, (fastener f.e. unit: Unit No. 20) ...
C  fastener for stringer number  2, (fastener f.e. unit: Unit No. 21) ...
C  fastener for stringer number  3, (fastener f.e. unit: Unit No. 22) ...
C  fastener for  ring   number  1, (Fastener f.e. unit: Unit No. 23) ...
C  fastener for  ring   number  2, (Fastener f.e. unit: Unit No. 24) ...
C  fastener for  ring   number  3, (Fastener f.e. unit: Unit No. 25) ...
```

Table 5 Part of the *.inp file concerned with edge conditions

```
(lines skipped to save space)
C Partial compatability (g-2) records for the cylindrical shell
 1   1 1 2 1   1 0 2 $ g-2 IU1,IR1,IC1,ID1,IU2,IR2,IC2,ID2;v=const.,row 1
 1   1 1 3 1   1 0 3 $ g-2 IU1,IR1,IC1,ID1,IU2,IR2,IC2,ID2;w=const.,row 1
 1   1 1 4 1   1 0 4 $ g-2 IU1,IR1,IC1,ID1,IU2,IR2,IC2,ID2;ru=const,row 1
 1  41 1 4 1  41 0 4 $ g-2 IU1,IR1,IC1,ID1,IU2,IR2,IC2,ID2;ru=const,row 41
 1  41 1 3 1  41 0 3 $ g-2 IU1,IR1,IC1,ID1,IU2,IR2,IC2,ID2;w=const.,row 41
 1 1   1 3 1 0   1 3 $ g-2 IU1,IR1,IC1,ID1,IU2,IR2,IC2,ID2;w=const.,col.1
 1 1  17 3 1 0  17 3 $ g-2 IU1,IR1,IC1,ID1,IU2,IR2,IC2,ID2;w=const.,col 17
C Partial compatability (g-2) records for stringer  1
   1   1   1 3   2   1   0 3 $ g-2 w=constant,row  1 (x=0) fayflg
   1  41   1 3   2  41   0 3 $ g-2 w=constant,row 41 (x=L) fayflg
   3   1   5 2   4   1   0 3 $ g-2 w=constant,row  1 outflange
   3  41   5 2   4  41   0 3 $ g-2 w=constant,row 41 outflange
C Partial compatability (g-2) records for stringer  2
   1   1   9 3   5   1   0 3 $ g-2 w=constant,row  1 fayflange
   1  41   9 3   5  41   0 3 $ g-2 w=constant,row 41 fayflg
   6   1   5 2   7   1   0 3 $ g-2 w=constant,row  1 outflg
   6  41   5 2   7  41   0 3 $ g-2 w=constant,row 41 outflg
C Partial compatability (g-2) records for stringer  3
   1   1  17 3   8   1   0 3 $ g-2 w=constant,row  1 fayflg
   1  41  17 3   8  41   0 3 $ g-2 w=constant,row 41 fayflg
   9   1   5 2  10   1   0 3 $ g-2 w=constant,row  1 outflg
   9  41   5 2  10  41   0 3 $ g-2 w=constant,row 41 outflg
C Partial compatability (g-2) records for ring  1
   1   1   1 3  11   0   1 3 $ g-2 w=constant,col  1 (y=0) fayflg
   1   1  17 3  11   0  17 3 $ g-2 w=constant,col 17 (y=Y) fayflg
  12   1   1 1  13   0   1 3 $ g-2 w=constant,col  1 outflg
  12   1  17 1  13   0  17 3 $ g-2 w=constant,col 17 outflg
C Partial compatability (g-2) records for ring  2
   1  21   1 3  14   0   1 3 $ g-2 w=constant,col  1 fayflg
   1  21  17 3  14   0  17 3 $ g-2 w=constant,col 17 fayflg
  15   1   1 1  16   0   1 3 $ g-2 w=constant,col  1 outflg
  15   1  17 1  16   0  17 3 $ g-2 w=constant,col 17 outflg
C Partial compatability (g-2) records for ring  3
   1  41   1 3  17   0   1 3 $ g-2 w=constant,col  1 fayflg
   1  41  17 3  17   0  17 3 $ g-2 w=constant,col 17 fayflg
  18   1   1 1  19   0   1 3 $ g-2 w=constant,col  1 outflg
  18   1  17 1  19   0  17 3 $ g-2 w=constant,col 17 outflg
C lagrange constraints to prevent stringer sidesway
C lagrange constraints to prevent  ring sidesway
C Lagrange constraints to impose linear variation of u at y=0
C Lagrange constraints to impose linear variation of u at y=YSTAGS
C Lagrange constraints to impose linear variation of v at y=0
C Lagrange constraints to impose linear variation of v at y=YSTAGS

C Begin unit 1: cylindrical shell
(lines skipped to save space)
C Input for boundary conditions...
 0  0  0  0  0 $ p-1 (IBLN(i), i=1,4), IBOND
 111  111    $ p-2 ITRA, IROT (boundary no. 1, x=0)
 111  111    $ p-2 ITRA, IROT (boundary no. 2, y=YSTAGS)
 101  111    $ p-2 ITRA, IROT (boundary no. 3, x=XSTAGS)
 111  111    $ p-2 ITRA, IROT (boundary no. 4, y=0)
```

Table 6 List of margins for an optimized imperfect Z-stiffened cylindrical shell with angle-ply skin and orthotropic stringers and rings, (Nx,Nxy)=(-700, +40) lb/in.

```
 MARGINS FOR CURRENT DESIGN: LOAD CASE NO. 1, SUBCASE NO. 1
 MAR. MARGIN
 NO.  VALUE               DEFINITION
 1  5.57E-01 Local buckling from discrete model-1.,M=6   axial halfwaves;FS=0.99
 2  8.70E-02 long-wave local buckling, discrete model(m=2   axial halfwav);FS=0.
 3  3.15E+01 fibertensn:matl=1,SKN,Dseg=1,node=1,layer=4,z=0.0141; MID.;FS=1.
 4  1.87E+01 fibercompr:matl=1,SKN,Dseg=1,node=1,layer=2,z=-0.0071; MID.;FS=1.
 5  1.82E+00 transcompr:matl=1,STR,Dseg=5,node=11,layer=1,z=-0.0141; MID.;FS=1.
 6  2.65E+00 inplnshear:matl=1,SKN,Dseg=1,node=1,layer=3,z=0.0071; MID.;FS=1.
 7  9.19E-01 fibercompr:matl=2,STR,Dseg=4,node=11,layer=1,z=-0.0234; MID.;FS=1.
 8  1.67E+01 transtensn:matl=2,SKN,Dseg=2,node=11,layer=1,z=0.05; MID.;FS=1.
 9  1.67E+01 transcompr:matl=2,SKN,Dseg=2,node=11,layer=1,z=-0.05; MID.;FS=1.
10  4.71E-01 (m=1   lateral-torsional buckling load factor)/(FS)-1;FS=0.999
11 -9.56E-04 Inter-ring bucklng, discrete model, n=10  circ.halfwaves;FS=0.999
12  2.67E+01 fibertensn:matl=1,SKN,Iseg=1,at:n=1,layer=4,z=0.0141;-MID.;FS=1.
13  2.06E+01 fibercompr:matl=1,SKN,Iseg=1,at:n=1,layer=3,z=0.0071;-MID.;FS=1.
14  1.43E+00 transcompr:matl=1,SKN,Iseg=1,at:n=1,layer=1,z=-0.0141;-MID.;FS=1.
15  2.12E+00 inplnshear:matl=1,SKN,Iseg=1,at:n=1,layer=2,z=-0.0071;-MID.;FS=1.
16  3.73E+00 fibertensn:matl=2,RNG,Iseg=4,allnode,layer=1,z=0.015;-MID.;FS=1.
17  9.39E-01 fibercompr:matl=2,STR,Iseg=4,allnode,layer=1,z=0.0234;-MID.;FS=1.
18  1.17E+02 transtensn:matl=2,SKN,Iseg=2,at:n=1,layer=1,z=-0.05;-MID.;FS=1.
19  1.17E+02 transcompr:matl=2,SKN,Iseg=2,at:n=1,layer=1,z=0.05;-MID.;FS=1.
20  1.59E+05 inplnshear:matl=2,SKN,Iseg=2,at:n=1,layer=1,z=0.05;-MID.;FS=1.
21  5.02E+00 buckling margin stringer Iseg.2 . Local halfwaves=80 .MID.;FS=1.
22  2.70E+00 buckling margin stringer Iseg.3 . Local halfwaves=14 .MID.;FS=1.
23  2.41E+00 buckling margin stringer Iseg.4 . Local halfwaves=14 .MID.;FS=1.
24  1.43E+00 buckling stringer Isegs.3+4 together.M=10 ;C=0.     ;MID.;FS=1.4
25  2.31E+01 buckling margin   ring   Iseg.3 . Local halfwaves=72 .MID.;FS=1.
26  6.26E+00 buckling margin   ring   Iseg.4 . Local halfwaves=66 .MID.;FS=1.
27  5.84E+00 buckling   ring   Isegs.3+4 together.M=50 ;C=0.     ;MID.;FS=1.4
28  9.25E-02 buck.(SAND);simp-support local buck.; (0.95*altsol);FS=0.999
29  3.52E-01 buck.(SAND);simp-support general buck;M=1;N=2;slope=50.;FS=0.999
30  2.27E-01 buck.(SAND);simp-support general buck;(0.85*altsol);FS=0.999
31  3.25E+00 buck.(SAND);rolling with smear rings; M=99;N=1;slope=0.03;FS=0.999
32  8.25E-01 buck.(SAND);rolling only of stringers;M=45;N=0;slope=0.;FS=1.6
33  6.48E-01 buck.(SAND);hiwave roll. of stringers;M=141;N=0;slope=0.;FS=1.98
34  8.80E+00 buck.(SAND);hiwave roll. of   rings;  M=0;N=51;slope=0.;FS=1.2
35  2.15E+01 buck.(SAND);rolling only axisym.rings;M=0;N=0;slope=0.;FS=1.6
36  2.76E+00 buck.(SAND); STRINGERS:  web buckling;M=15;N=1;slope=0.03;FS=1.
37  2.89E+01 buck.(SAND);   RINGS:    web buckling;M=66;N=1;slope=0.6546;FS=1.
38  2.54E+02 (Max.allowable ave.axial strain)/(ave.axial strain) -1; FS=1.
39  5.28E+00 0.3333 *(Stringer spacing, b)/(Stringer base width, b2)-1;FS=1.
40  2.56E+01 1.     *(Ring spacing, b)/(Ring base width, b2) -1; FS=1.
```

Table 7 Design variables used in this study

```
VAR. NO.                          DEFINITION
   1      B(STR):stiffener spacing, b: STR seg=NA, layer=NA  (stringer spacing)
   2     B2(STR):width of stringer base, b2 (must be > 0)
   3      H(STR):height of stiffener (type H for sketch), h  (see Fig. 5a)
   4      W(STR):width of outstanding flange of stiffener, w
   5   T(1)(SKN):thickness for layer index no.(1 ): STR seg=1 (panel skin)
   6 ANG(1)(SKN):winding angle (deg.) for layer index no.(1 ) (panel skin)
   7   T(2)(SKN):thickness for layer index no.(2 ): STR seg=1 (panel skin)
   8 ANG(2)(SKN):winding angle (deg.) for layer index no.(2 ) (panel skin)
   9   T(3)(STR):thickness for layer index no.(3 ): STR seg=2 (stringer faying flange)
  10   T(4)(STR):thickness for layer index no.(4 ): STR seg=3 (stringer web)
  11   T(5)(STR):thickness for layer index no.(5 ): STR seg=4 (stringer outst. flange)
  12      B(RNG):stiffener spacing, b: RNG seg=NA, layer=NA   (ring spacing)
  13     B2(RNG):width of ring base, b2 (zero is allowed)
  14      H(RNG):height of stiffener (type H for sketch), h
  15      W(RNG):width of outstanding flange of stiffener, w
  16   T(6)(RNG):thickness for layer index no.(6 ): RNG seg=2 (ring faying flange)
  17   T(7)(RNG):thickness for layer index no.(7 ): RNG seg=3 (ring web)
  18   T(8)(RNG):thickness for layer index no.(8 ): RNG seg=4 (ring outst. flange)
```

Table 8 Starting design and optimum designs of perfect and imperfect ring and stringer stiffened cylindrical shells obtained via PANDA2

VAR. NO.	Decision Variable (Table 7)	Starting Design (in.,deg.)	O P T I M U M D E S I G N S (inches or deg.) P E R F E C T			I M P E R F E C T		
			Blade	Tee	Zee	Blade	Tee	Zee
1	B(STR)	4.0	1.885	1.885	1.885	1.885	1.885	1.885
2	B2(STR)	0.2	0.6283	0.1376	0.100	0.6283	0.100	0.100
3	H(STR)	0.5	0.1417	0.1000	0.1322	0.2272	0.2145	0.1440
4	W(STR)	0.3	----	0.1000	0.100	----	0.1769	0.100
5	T(1)(SKN)	0.01	0.006263	0.006270	0.00626	0.006704	0.006617	0.007055
6	ANG(1)(SKN)	45.0	70.00	70.00	69.92	69.307	70.000	69.830
7	T(2)(SKN)	0.01	0.006263	0.006270	0.00626	0.006704	0.006617	0.007055
8	ANG(2)(SKN)	-45.0	-70.00	-70.00	-69.92	-69.307	-70.00	-69.830
9	T(3)(STR)	0.1	-------	0.0300	0.06304	------	0.06703	0.100
10	T(4)(STR)	0.1	0.08194	0.04489	0.04618	0.09136	0.03677	0.04041
11	T(5)(STR)	0.1	-------	0.05674	0.03399	------	0.03248	0.04676
12	B(RNG)	7.0	4.00	4.00	4.00	4.00	4.00	4.00
13	B2(RNG)	0.2	0.00	0.100	0.18805	0.00	0.100	0.15037
14	H(RNG)	0.5	0.1595	0.13326	0.15957	0.13109	0.10302	0.14864
15	W(RNG)	0.3	-------	0.100	0.11664	------	0.100	0.100
16	T(6)(RNG)	0.1	-------	0.03035	0.03408	------	0.03422	0.03062
17	T(7)(RNG)	0.1	0.03202	0.0300	0.0300	0.03255	0.0300	0.0300
18	T(8)(RNG)	0.1	-------	0.03260	0.03502	------	0.0300	0.0300
Weight(180 deg.;lbs)=			2.120	2.306	2.367	2.548	2.600	2.693

Fixed properties:
 length of shell, L = 60 in.; Radius = 6.0 in.; b.c.= classical simple support
 shell wall is 4-layered angle-ply: [angle,-angle,-angle,angle] with each
 layer equal in thickness to T(1) and "angle" = ANG(1), Material No. 1.
 stiffener segments: all of Material No. 2, one-layered orthotropic
 amplitude of initial general buckling modal imperfection: Wimp=0.025 in.
 amplitude of inter-ring buckling modal imperfection = 0.0
 amplitude of local skin buckling modal imperfection = 0.0

Material Properties and allowables:
 Material No. 1: (E1=13.75, E2=1.03, G12=0.42, Nu=0.25, G13=G23=0.42)x10**6 psi
 Weight density = 0.057 lb/in**3; no thermal expansion
 Material No. 2: (E1=14.0, E2=1.04, G12=0.40, Nu=0.24, G13=G23=0.40)x10**6 psi
 Weight density = 0.060 lb/in**3; no thermal expansion

 Maximum stress allowables for both Material No. 1 and Material No. 2:
 Max. tension along fibers = 140000; Max. compression along fibers = 120000 psi
 Max. tension normal to fibers=10000; Max. compression normal to fibers=10000
 Maximum in-plane shear = 5000 psi

Bounds on decision variables (inches or degrees); linking (T(2),ANG(2)):
 1.885<B(STR)<6.283; 0.1<B2(STR)<0.4; 0.1<H(STR)<1.0; 0.1<W(STR)<0.5;
 0.005<T(1)(SKN)<0.1; 20.0<ANG(1)(SKN)<70; T(2) = T(1); ANG(2) = -ANG(1);
 0.03<T(3)(STR)<0.1; 0.03<T(4)(STR)<0.1; 0.03<T(5)(STR)<0.1
 4.0<B(RNG)<12; 0.1<B2(RNG)<0.4; 0.1<H(RNG)<1.0; 0.1<W(RNG)<0.4;
 0.03<T(4)(RNG)<0.1; 0.03<T(5)(RNG)<0.1; 0.03<T(6)(RNG)<0.1
Linked variables: T(2) = T(1); ANG(2) = -ANG(1); and,
 for blades without faying flanges only: B2(STR)=0.3333*B(STR)

Two load cases, both involving axial compression Nx and in-plane shear Nxy:
 Case 1: (Nx, Nxy) = (-700, +40); Case 2: (Nx, Nxy) = (-100,+150) lb/in.

Table 9 List of the most critical margins from all PANDA2 cases

Margin number	DEFINITION OF MARGIN
1	Local buckling from discrete model-1.,M=9 axial halfwaves;FS=0.99
2	long-wave local buckling, discrete model(m=2 axial halfwav);FS=0.
3	(m=1 lateral-torsional buckling load factor)/(FS)-1;FS=0.999
4	Inter-ring bucklng, discrete model, n=10 circ.halfwaves;FS=0.999
5	Lo-n Inter-ring buck.,discrete model,n=1 circ.halfwaves;FS=0.999
6	Long-axial-wave bending-torsion buckling; M=1 ;FS=0.999
7	buckling margin stringer Iseg.3 . Local halfwaves=2 .MID.;FS=1.
8	buckling margin stringer Iseg.4 . Local halfwaves=9 .MID.;FS=1.
9	buckling stringer Isegs.3+4 together.M=9 ;C=0. ;MID.;FS=1.4
10	buckling stringer Iseg 4 as beam on foundation. M=16 ;MID.;FS=3.
11	buck.(SAND);simp-support local buck.; (0.95*altsol);FS=0.999
12	buck.(SAND);simp-support general buck;M=1;N=2;slope=100.;FS=0.999
13	buck.(SAND);simp-support general buck;(0.85*altsol);FS=0.999
14	buck.(SAND);rolling with smear rings; M=129;N=1;slope=0.03;FS=0.999
15	buck.(SAND);rolling only of stringers;M=139;N=0;slope=0.;FS=1.6
16	buck.(SAND);hiwave roll. of stringers;M=145;N=0;slope=0.;FS=1.2
17	transcompr:matl=1,SKN,Dseg=2,node=6,layer=4,z=0.0125; MID.;FS=1.
18	fibercompr:matl=2,STR,Dseg=3,node=1,layer=1,z=0.041; MID.;FS=1.
19	transcompr:matl=1,SKN,Iseg=2,at:n=6,layer=4,z=0.0125;-MID.;FS=1.
20	fibercompr:matl=2,STR,Iseg=3,at:ROOT,layer=1,z=0.;-MID.;FS=1.
21	0.3333 *(Stringer spacing, b)/(Stringer base width, b2)-1;FS=1.

Table 10 Values of the most critical margins from PANDA2 for Load Set No. 1: (Nx,Nxy)=(-700,+40) lb/in

Margin Number	VALUES OF MARGINS AT OPTIMUM DESIGNS											
	Perfect Blade		Imperfect Blade		Perfect Tee		Imperfect Tee		Perfect Zee		Imperfect Zee	
	2 subcases:		2 subcases:		2 subcases:		2 subcases:		2 subcases:		2 subcases:	
	1	2	1	2	1	2	1	2	1	2	1	2
1	0.055	0.031	0.727	0.776	0.456	0.506	0.732	0.768	0.529	0.590	0.557	0.646
2	0.277	-0.048	0.563	0.413	0.762	0.126			0.179	0.001	0.087	-.004
3	0.446	0.127		0.709		0.375	0.340	0.176		0.191	0.471	0.179
4	0.184	0.184			0.208	0.211			-.003	-.003	-.001	0.014
5	0.984	0.984										
6							0.302	0.117				
7	0.471	0.372	0.073	0.034								
8							0.568	0.427		0.740		
9							0.534	0.419		0.764		
10					0.144	-.003	0.096	-.003				
11	0.088	0.007	0.164	0.230	0.258	0.014	0.274	0.086	0.315	0.016	0.093	-.012
12	0.011		0.279		0.231		0.658		0.234		0.352	
13	0.011		0.653		0.071		0.113		0.015		0.227	
14	0.693	0.767										
15	0.754	0.591			0.547	0.399	0.093	0.016	0.763	0.571	0.825	0.684
16							0.926	0.794		0.155	0.648	0.532
17	0.669				0.941							
18	0.354				0.576	0.457		0.949	0.704	0.572	0.919	0.769
19	0.669				0.916	0.950						
20	0.354				0.562	0.360			0.702	0.497	0.939	0.752
21	0.000		0.000									

Table 11 Values of the most critical margins from PANDA2 for Load Set No. 2: (Nx,Nxy)=(-100,+150) lb/in

Margin Number	VALUES OF MARGINS AT OPTIMUM DESIGNS											
	Perfect Blade		Imperfect Blade		Perfect Tee		Imperfect Tee		Perfect Zee		Imperfect Zee	
	2 subcases:		2 subcases:		2 subcases:		2 subcases:		2 subcases:		2 subcases:	
	1	2	1	2	1	2	1	2	1	2	1	2
1	0.531	0.551			0.436	0.881			0.399	0.932	0.695	
2	0.790	0.390	0.608	0.574			0.470	0.470				
3												
4												
5									0.889			
6												
7												
8												
9												
10												
11	0.001	-0.011	0.002	-.009	0.014	-.001	0.014	0.005	0.014	-.002	0.180	0.171
12	0.085		0.314		0.290		0.903		0.264		0.916	
13	0.311		0.819		0.280		0.664		0.438		0.955	

Table 12 Predictions from PANDA2 for general buckling of panels with three near-optimum designs that differ little from each other

general buckling (180-degree panel weight = 2.548 lbs, Design No. 1)						
EIGMNC=	2.08E+00	2.08E+00	2.11E+00	2.29E+00	2.11E+00	2.08E+00
SLOPEX=	2.28E-01	2.28E-01	0.00E+00	0.00E+00	0.00E+00	2.28E-01
MWAVEX=	1	1	6	13	6	1
NWAVEX=	4	4	5	7	5	4
general buckling (180-degree panel weight=2.547, Design No. 2)						
EIGMNC=	2.36E+00	2.36E+00	2.32E+00	2.47E+00	2.32E+00	2.32E+00
SLOPEX=	2.28E-01	2.28E-01	0.00E+00	0.00E+00	0.00E+00	0.00E+00
MWAVEX=	1	1	7	13	7	7
NWAVEX=	4	4	5	7	5	5
general buckling (180-degree panel weight = 2.572 lbs, Design No. 3)						
EIGMNC=	2.36E+00	2.36E+00	2.27E+00	1.00E+17	2.27E+00	2.27E+00
SLOPEX=	2.28E-01	2.28E-01	0.00E+00	0.00E+00	0.00E+00	0.00E+00
MWAVEX=	1	1	10	0	10	10
NWAVEX=	4	4	6	0	6	6

NOTE: EIGMNC = eigenvalue (buckling load factor); SLOPEX = slope of the buckling nodal lines; MWAVEX = number of axial halfwaves in the buckling mode: NWAVEX = number of circumferential halfwaves in the buckling mode. The PANDA2 model of the cylindrical shell spans 180 degrees [1].

Table 13 Characteristics of STAGS models used in this study

STAGS model number	Main characteristics of STAGS model and sub-characteristics of STAGS model
	Main characteristics of STAGS model
0	one bay, panel skin only, classical simple support on all four edges; prespecified pure membrane prebuckling state: (Nx, Nxy)
1	one bay: X x Y = 4.0 x 1.885 in., panel skin with stringers and rings replaced by constraints w = const along all four edges or with half-stiffness stringers and rings along the edges (Fig. 16)
2	3 bays x 3 bays: X x Y = 12.0 x 5.655 in., panel skin with 4 stringers and 4 rings, nodal mesh concentrated in center bay.(Fig.17)
3	4 bays x 8 bays: X x Y = 16.0 x 15.08 in., panel skin with 9 stringers and 5 rings, 8 nodal points between stringers, 20 nodal points between rings, (Fig.18)
4	4 bays between rings x 360 deg. of circumference, panel skin with 20 stringers and 5 rings, 8 nodal points between stringers, 20 nodal points between rings. (Fig.19)
5	entire shell: 60 inches long x 360 deg. of circumference, panel skin with 20 stringers and 15 rings, rings not at edges, nodal point spacing varies along x as shown in Fig.20
6	same as 5 except: 1. rings at ends (16 rings); 2. uniform grid spacing with 6 nodal points between stringers and 20 between rings.
	Sub-characteristics of STAGS model
a	480 finite elements
b	410 finite elements
c	with fasteners
d	without fasteners
e	edge sidesway of stiffeners prevented
f	edge sidesway of stiffeners permitted
g	in-plane warping of two straight edges prevented
h	in-plane warping of two straight edges permitted
i	stringers are modeled entirely with shell units
j	stringer web and outstanding flange are shell units, faying flange is modeled as a discrete beam (210 elements)
k	stringer web is a shell unit, faying flange and outstanding flange are modeled as discrete beams (210 elements)
l	stringers are modeled entirely as discrete beams (210 elements)
m	stringers are modeled as lines where normal displacement w = 0
n	stringers are smeared out in the manner of Baruch and Singer [28]
o	rings are modeled entirely with shell units
p	ring web and outstanding flange are shell units, faying flange is modeled as a discrete beam (210 elements)
q	ring web is a shell unit, faying flange and outstanding flange are modeled as discrete beams (210 elements)
r	rings are modeled entirely as discrete beams (210 elements)
s	rings are modeled as lines where normal displacement w = 0
t	rings are smeared out in the manner of Baruch and Singer [28]
u	load set no. 1: Nx = -700 lb/in, Ny = 0, Nxy = +40 lb/in.
v	load set no. 2: Nx = -100 lb/in, Ny = 0, Nxy = +150 lb/in.

Table 14 Characteristics of STAGS buckling modes found during this study

STAGS buckling mode number	Characteristics of STAGS buckling mode
1	skin buckling only (Fig.16a-c)
2	primarily skin buckling with some stiffener rolling (Fig.17)
3	primarily stiffener rolling with some skin buckling (Fig. 3)
4	primarily inter-ring buckling with minor deflection of some of the stringer roots (Fig. 19)
5	primarily inter-ring buckling with major deflection of some of the stringer roots (Figs. 20 - 22)
6	general instability with considerable local deformation (Fig. 23)
7	general instability with minor local deformation (Fig. 24)
8	pure general instability (Fig. 25)
9	edge buckling (Fig. 26)

Table 15 Buckling load factors of the skin of the Blade-stiffened cylindrical shells

STAGS model (Table 13)	Buckling mode (Table 14)	BUCKLING LOAD FACTORS from STAGS model	from PANDA2 Stringer segment	Lateral torsion	Local skin	Inter-ring	General buckling
Optimized perfect (half-weight=2.120 lbs)			PANDA2 RESULTS				
			Load 1->1.372	0.952	1.007	1.011	1.011(n=2)
			Load 2->8.68	1.390	0.990	1.311	1.085(n=3)
0,a,u	1	1.100(m=8 halfwaves between rings)					
0,a,v	1	1.037(m=3 halfwaves between rings)					
1,a,d,e,h,i,o,u	1	1.066(m=1 halfwaves between rings)					
1,a,d,e,g,i,o,u	1	1.203(m=10 halfwaves between rings)					
1,a,d,e,h,m,s,u	1	0.831(m=1 halfwaves between rings)					
1,a,d,e,g,m,s,u	1,9	0.957("quanset hut" buckling mode between rings)-Fig. 16a,c					
1,a,d,e,g,m,s,u	1	1.184(m=8 halfwaves between rings; 2nd eigenvalue)–Fig. 16b					
1,a,d,e,h,i,o,v	1	1.146(m=1 halfwaves between rings)					
1,a,d,e,g,i,o,v	1	1.345(m=6 halfwaves between rings)					
1,a,d,e,h,m,s,v	1	0.974(m=1 halfwaves between rings)					
1,a,d,e,g,m,s,v	1	1.255(m=6 halfwaves between rings)					
2,a,d,e,g,i,o,u	1	1.189(m=8 halfwaves between rings)					
2,a,d,e,h,i,o,u	1	1.160(m=8 halfwaves between rings, 12th root)					
2,a,d,e,g,i,o,v	2	1.312(m=6 halfwaves between rings)					
2,a,d,e,h,i,o,v	2	1.263(m=4 halfwaves between rings)-Fig. 17					

Table 16 Buckling load factors of the Blade-stiffened cylindrical shells

STAGS model (Table 13)	Buckling mode (Table 14)	BUCKLING LOAD FACTORS from STAGS model	from PANDA2 Stringer segment	Lateral torsion	Local skin	Inter-ring	General buckling
Optimized perfect (half-weight=2.120 lbs)			PANDA2 RESULTS				
			Load 1->1.372	0.952	1.007	1.011	1.011(n=2)
			Load 2->8.68	1.390	0.990	1.311	1.085(n=3)
3,a,c,e,g,i,o,u	5	0.975					
4,a,d,e,-,i,o,u	5	0.964					
4,a,c,e,-,i,o,u	5	0.961					
5,a,d,f,-,i,o,u	5	0.978 – Figs. 20, 21, 22					
5,a,d,f,-,i,o,u	6	1.129(n=3, 88th mode) - Fig. 23					
5,a,d,f,-,i,o,u	7	1.143(n=2, 96th mode) – Fig. 24					
3,a,d,e,g,i,o,v	4,5	1.089					
3,a,c,e,g,i,o,v	4,5	1.100					
5,a,d,f,-,i,o,v	4,5	1.064 (1st mode)					
5,a,d,f,-,i,o,v	7	1.211(n=3, 58th mode)					
5,b,d,f,-,i,o,v	8	1.268(n=3, 1st mode)					
5,b,d,f,-,i,o,v	8	1.359(n=4, 3rd mode)					
5,b,d,f,-,i,o,v	4,5	1.391 (5th mode)					
5,b,c,f,-,i,o,v	8	1.242(n=3, 1st mode)					
6,b,c,f,-,i,o,v	4,5	1.109 (1st mode)					
Optimized imperfect (half-weight=2.548 lbs)							
Imperfection amplitude, Wimp = 0.0			PANDA2 RESULTS				
			Load 1-> 1.046	1.864	1.526	1.869	1.636(n=2)
			Load 2->19.1	14.9	1.19	1.981	1.378(n=4)
3,a,d,e,g,i,o,u	5	1.763					
4,a,d,e,-,i,o,u	4,5	1.765					
5,a,d,f,-,i,o,u	8	1.562(n=3, 1st and 2nd modes (modes in pairs))-Fig. 25					
5,a,d,f,-,i,o,u	7	1.625(n=4, 3rd and 4th modes)					
5,a,d,f,-,i,o,u	8	1.646(n=2, 5th and 6th modes)					
5,a,d,f,-,i,o,u	4,5	1.785 (ninth mode)					
3,a,d,e,g,i,o,v	4,5	1.503					
4,a,d,e,-,i,o,v	4	1.486					
4,a,d,f,-,i,o,v	4	1.483					
5,a,d,f,-,i,o,v	7,8	1.300(n=4, 1st mode)					
5,a,d,f,-,i,o,v	8	1.314(n=3, 3rd mode)					
5,a,d,f,-,i,o,v	7	1.464(n=5, 5th mode)					
5,a,d,f,-,i,o,v	4,5	1.485 (7th mode)					
Optimized imperfect (half-weight=2.548 lbs)		Imperfection used in PANDA2: Wimp(general)=0.025 in.					
			Load 1->1.034	1.413	1.164	1.653	1.279(n=2)
			Load 2->6.91	1.574	0.991	1.819	1.314(n=4)
Imperfections used in STAGS:		Imperfection amplitude, Wimp(general)=various					
		Imperfection amplitude, Wimp(panel)=various					
4,a,d,f,-,i,o,u	2	1.159 (Wimp(general)=0., Wimp(panel)=0.01 in.)-Fig. 40					
5,a,d,f,-,i,o,u	7	1.126 (Wimp(general)=0.025(n=3),Wimp(panel)=0.01 in.)					
5,a,d,f,-,i,o,u	7	1.361 (Wimp(gen)=0.025(n=3),Wimp(panel)=.0001 in.)-Fig. 29					
5,a,d,f,-,i,o,u	2	1.087 (Wimp(gen)=0.025(n=4),Wimp(panel)=0.01in.-Figs.40,27,28					
4,a,d,f,-,i,o,v	2	1.050 (Wimp(general)=0., Wimp(panel)=0.01 in.)-Fig. 40					
5,a,d,f,-,i,o,v	2	1.087 (Wimp(general)=0.025(n=4),Wimp(panel)=0.01 in.)-Fig. 40					

Table 17 Buckling load factors of the Tee-stiffened cylindrical shells

STAGS model (Table 13)	Buckling mode (Table 14)	BUCKLING LOAD FACTORS from STAGS model	from PANDA2: Stringer segment	Lateral torsion	Local skin	Inter-ring	General buckling
Optimized perfect (half-weight=2.306 lbs)		PANDA2 RESULTS					
		Load 1->0.997	1.126	1.014	1.071	1.231(n=2)	
		Load 2->7.05	9.44	0.999	1.280	1.290(n=3)	
2,a,c,e,g,i,o,u	1	1.385(m=8 halfwaves between rings)					
3,a,c,e,g,i,o,u	5	1.088					
2,a,c,e,g,i,o,v	1	1.337(m=7 halfwaves between rings)					
3,a,d,e,g,i,o,v	4,5	1.148					
3,a,c,e,g,i,o,v	4,5	1.155					
Optimized imperfect (half-weight=2.600 lbs)							
Imperfection amplitude, Wimp = 0.0		PANDA2 RESULTS					
		Load 1->0.997	1.020	1.389	1.197	1.967(n=2)	
		Load 2->7.00	7.16	1.150	1.734	1.973(n=3)	
2,b,d,e,g,l,r,u	1	1.979(m=8 halfwaves between rings)					
2,b,d,e,g,m,s,u	1	1.812(m=8 halfwaves between rings)					
3,b,d,e,g,i,o,u	3	1.200(m=6 halfwaves over 4 bays)					
3,b,c,e,g,i,o,u	2,3	1.448(m=6 halfwaves over 4 bays)					
3,b,c,e,g,j,p,u	2,3	1.520(m=6 halfwaves over 4 bays)					
3,b,d,e,g,k,q,u	9	1.650					
3,a,d,e,g,i,o,u	3	1.170(m=6 halfwaves over 4 bays)					
3,a,c,e,g,i,o,u	2,3	1.410(m=6 halfwaves over 4 bays)					
3,a,c,e,h,i,o,u	2,3	1.334(m=5 halfwaves over 4 bays)					
3,a,d,e,g,i,t,u	3	1.417 (m=7; entirely stringer rolling without skin.)					
3,a,c,f,g,i,o,u	9	0.960					
4,b,c,e,-,j,p,u	2,3	1.473(m=6 halfwaves over 4 bays)					
4,a,c,e,-,i,o,u	2,3	1.360(m=5 halfwaves over 4 bays)-Fig. 19a					
5,a,d,e,-,n,t,u	8	2.443(n=2, 1st mode)					
5,b,d,e,-,n,t,u	8	2.496(n=2, 1st mode)					
5,b,d,e,-,l,r,u	8	2.427(n=2, 1st mode)					
5,a,d,e,-,n,o,u	8	2.303(n=2, 1st mode)					
5,a,d,e,-,i,t,u	-	cannot find general mode: 760 local modes hide it.					
3,a,c,e,g,i,o,v	2,3	1.572					
4,a,c,e,-,i,o,v	2,3,4	1.533(m=5 halfwaves over 4 bays)					
5,a,d,e,-,i,t,v	8	2.614(n=3)					
5,a,c,e,-,i,t,v	8	2.587(n=3)					
Optimized imperfect (half-weight=2.600 lbs)		Imperfection used in PANDA2: Wimp(general)=0.025 in.					
		Load 1->0.997	1.016	1.086	1.113	1.658(n=2)	
		Load 2->7.01	1.470	1.005	1.664	1.903(n=3)	
Imperfections used in STAGS: Imperfection amplitude, Wimp(general)=various Imperfection amplitude, Wimp(panel)=various							
3,a,d,e,g,i,o,u	2,3	0.899 (Wimp(general)=0., Wimp(panel)=0.01 in.)-Fig. 34					
3,b,d,e,g,i,o,u	2,3	0.901 (Wimp(general)=0., Wimp(panel)=0.01 in.)-Fig. 34					
3,a,c,e,g,i,o,u	2,3	0.905 (Wimp(general)=0., Wimp(panel)=0.01 in.)-Fig. 34					
3,b,c,e,g,i,o,u	2,3	0.940 (Wimp(general)=0., Wimp(panel)=0.01 in.)-Fig. 34					
3,b,c,e,g,j,p,u	2,3	0.970 (Wimp(general)=0., Wimp(panel)=0.01 in.)-Fig. 34					
3,b,d,e,g,k,q,u	9	1.092 (Wimp(general)=0., Wimp(panel)=0.01 in.)-Fig. 34					
2,b,d,e,g,l,r,u	1	1.75 (Wimp(general)=0., Wimp(skin)=0.01 in.)-Fig. 34					
2,a,d,e,g,m,s,u	1	1.18 (Wimp(general)=0., Wimp(skin)=0.01 in.)-Fig. 34					
4,b,c,e,-,j,p,u	2,3	0.990 (Wimp(general)=0., Wimp(panel)=0.01 in.)					
4,a,c,e,-,i,o,u	2,3	0.920 (Wimp(general)=0., Wimp(panel)=0.01 in.)-Figs. 40,19b,34					
3,a,c,f,g,i,o,u	9	0.800 (Wimp(general)=0., Wimp(panel)=0.01 in.)-Fig. 26					
3,a,c,e,h,i,o,u	2,3	0.890 (Wimp(general)=0., Wimp(panel)=0.01 in.)-Fig. 34					
3,a,c,e,g,i,o,v	2	0.940 (Wimp(general)=0., Wimp(panel)=0.01 in.)					
4.a,c.e.-.i.o,v	2	0.940 (Wimp(general)=0., Wimp(panel)=0.01 in.)-Fig. 40					

Table 18 Buckling load factors of the Zee-stiffened cylindrical shells

STAGS model (Table 13)	Buckling mode (Table 14)	BUCKLING LOAD FACTORS from STAGS model	from PANDA2 Stringer segment	Lateral torsion	Local skin	Inter-ring	General buckling
Optimized perfect (half-weight=2.367 lbs)			PANDA2 RESULTS				
			Load 1-> 1.740	1.001	1.016	0.997	1.234(n=2)
			Load 2->12.3	8.23	0.998	1.438	1.264(n=3)
2,a,c,e,g,i,o,u	1	1.467(m=7 halfwaves between rings)					
3,a,c,e,g,i,o,u	5	1.110					
3,a,d,e,g,i,o,u	5	0.984					
3,b,d,e,h,i,o,u	5	1.056					
2,a,c,e,g,i,o,v	1	1.349(m=5 halfwaves between rings)					
3,a,c,e,g,i,o,v	5	1.172					
Optimized imperfect (half-weight=2.693 lbs)							
Imperfection amplitude, Wimp = 0.0			PANDA2 RESULTS				
			Load 1-> 2.19	1.690	1.621	1.163	1.961(n=2)
			Load 2->15.4	11.3	1.331	2.03	1.976(n=3)
1,a,d,e,g,m,s,u	1	1.767("quanset hut" mode between rings, mode 1)					
1,a,d,e,g,m,s,u	1	2.044(m=8, halfwaves between rings, mode 2)					
1,a,c,f,g,i,o,u	3,9	1.511					
1,a,c,e,g,i,o,u	3	1.968(m=3 halfwaves between rings)					
3,a,d,e,g,i,o,u	5	1.386(m=6 halfwaves over four bays)					
3,a,c,e,g,i,o,u	5	1.528 (Fig. 18)					
4,a,c,e,-,i,o,u	5	1.501(m=6 halfwaves over four bays)					
5,b,d,e,-,l,r,u	8	2.992(n=2, crude mesh: one 410 element/bay)					
5,a,d,e,-,n,o,u	8	2.275(n=2, crude mesh: one 480 element/bay)					
1,a,d,e,g,m,s,v	1	1.714(m=6 halfwaves between rings)					
1,a,c,f,g,i,o,v	1	1.867(m=6 halfwaves between rings)					
3,a,c,e,g,i.o.v	5	1.579					
4,a,c,e,-,i,o,v	2,3,4	1.530					
5,a,d,e,-,n,t,v	8	3.115(n=3)(uniform mesh: 101 x 121 nodal points)					
5,b,d,e,-,n,t,v	8	3.151(n=3)(uniform mesh: 101 x 121 nodal points)					
5,b,d,e,-,l,r,v	8	2.954(n=3)(uniform mesh: 45 x 41 nodal points					
5,a,d,e,-,i,t,v	8	3.110(n=3)(uniform mesh: 101 x 121 nodal points)					
5,a,d,e,-,i,o,v	4,5	1.564 (six 480 elements/bay in middle 7 bays)					
5,a,d,e,-,i,o,v	7	2.096(n=3, six 480 elements/bay in middle 7 bays)					
5,a,d,e,-,i,o,v	6	2.079(n=3, 12 480 elements/bay in middle 3 bays)					
Optimized imperfect (half-weight=2.693 lbs)							
		Imperfection used in PANDA2: Wimp(general)=0.025 in.					
			Load 1-> 2.19	0.996	0.988	0.999	1.352(n=2)
			Load 2->15.4	1.695	1.171	1.955	1.916(n=3)
Imperfections used in STAGS:		Imperfection amplitude, Wimp(general)=various					
		Imperfection amplitude, Wimp(panel)=various					
3,a,d,e,g,i,o,u	5	0.900 (Wimp(general)=0., Wimp(panel)=0.01 in.)-Fig. 35					
3,a,c,e,g,i,o,u	5	0.980 (Wimp(general)=0., Wimp(panel)=0.01 in.)-Fig. 35					
4,a,c,e,-,i,o,u	5	0.976 (Wimp(general)=0., Wimp(panel)=0.01 in.)-Fig. 40					
3,a,c,e,g,i,o,v	2	1.02 (Wimp(general)=0., Wimp(panel)=0.01 in.)					
4,a,c,e,-,i,o,v	2,4	0.97 (Wimp(general)=0., Wimp(panel)=0.01 in.)-Fig. 40					
5,various,v		See Figs. 36-38					

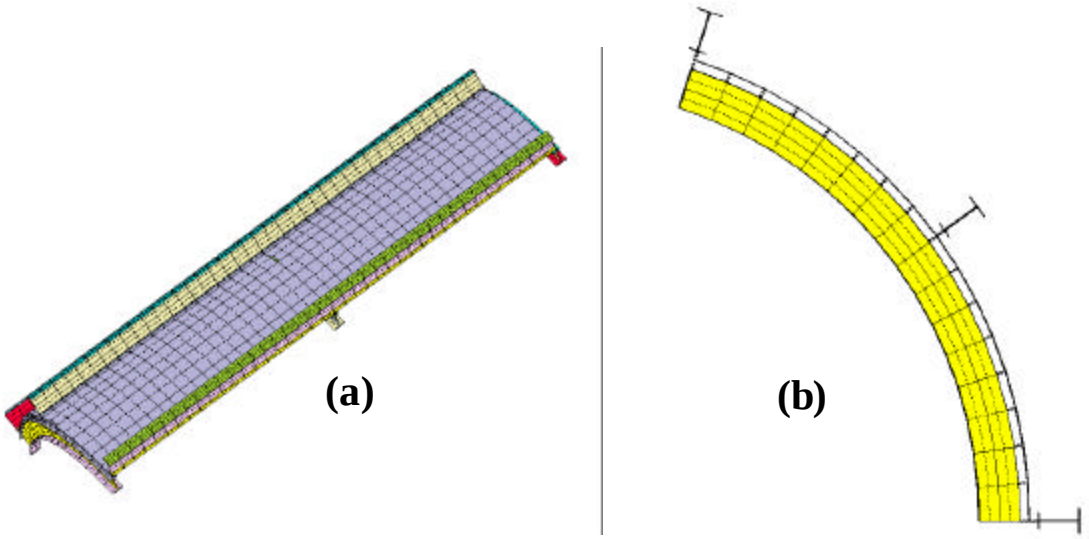

Fig. 1 STAGS model generated with STAGSUNIT for a starting design

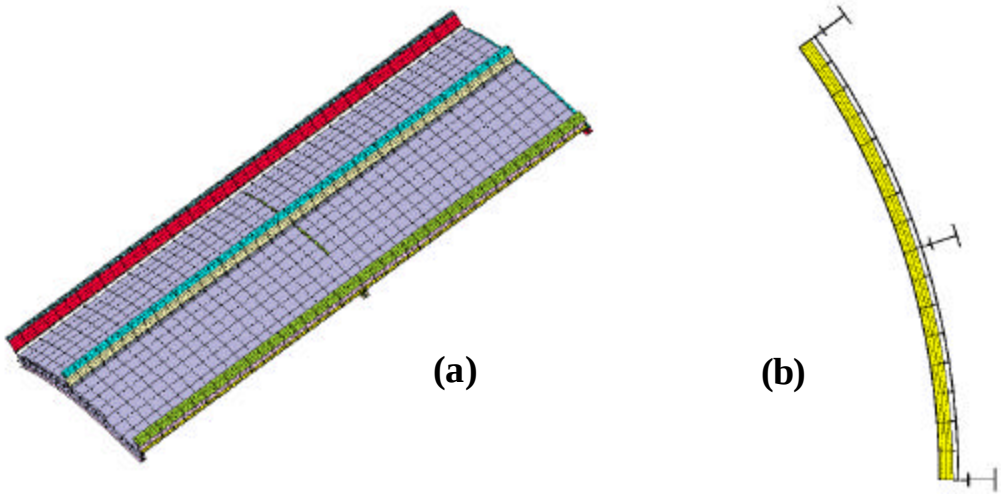

Fig. 2 STAGS model for the optimized design

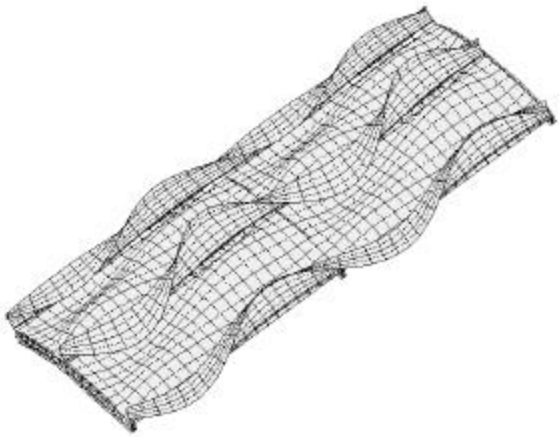

Fig. 3 Bifurcation buckling of the optimized design under Load Set 1

Fig. 4 The rare buckling mode in which normal buckling modal displacement *w* is largest and constant along a boundary.

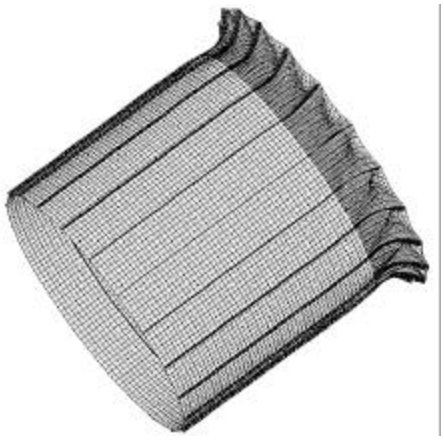

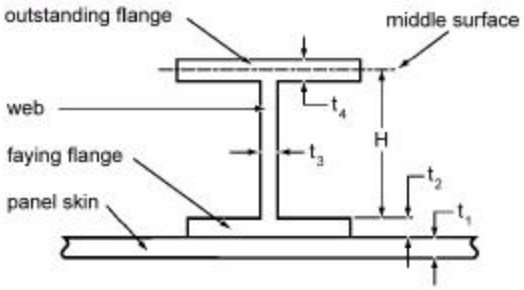

Fig. 5a Actual stiffener

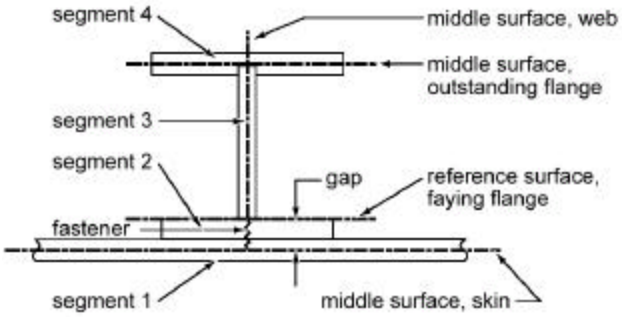

Fig. 5b Model with fasteners

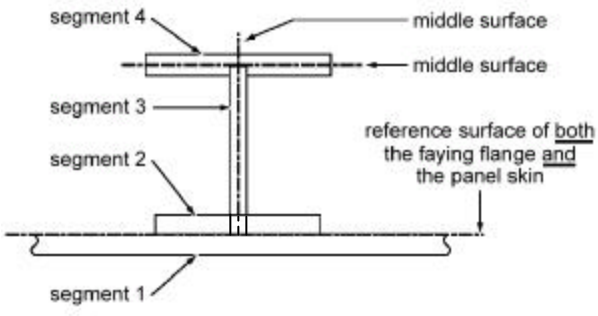

Fig. 5c Model without fasteners

Fig. 5 Locations of reference surfaces in STAGS models with and without fasteners

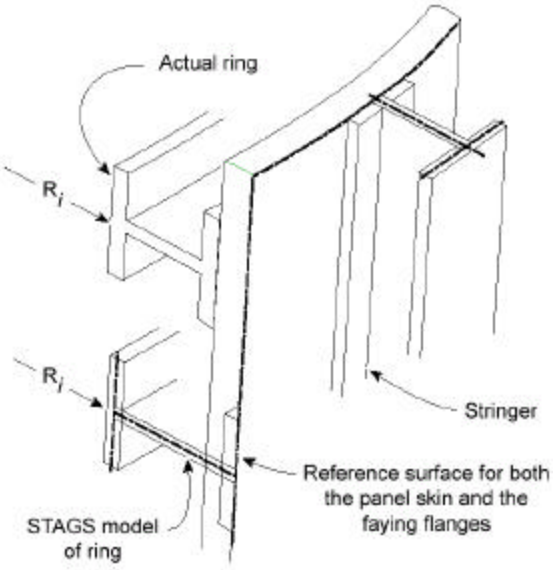

Fig. 6 STAGS models when there are no fasteners, showing rings and stringer

Fig. 7 A spurious buckling mode in the STAGS model with 410 elements.

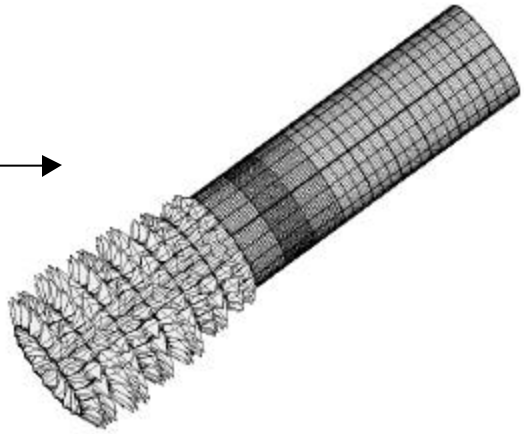

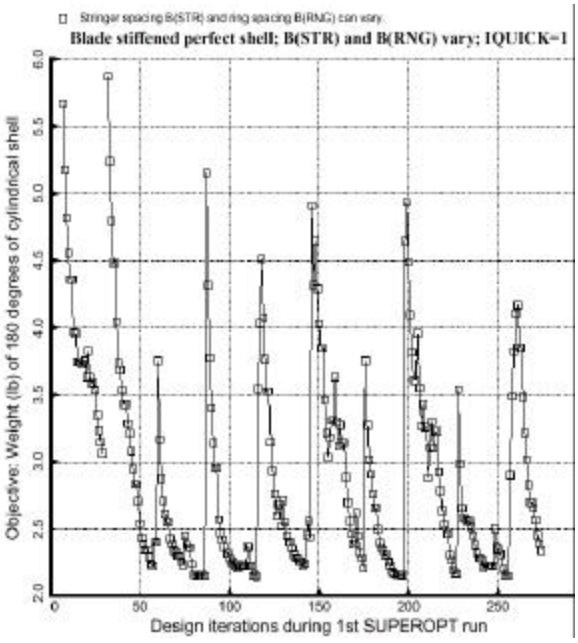

Fig. 8 Objective vs. design iterations from PANDA2 with IQUICK = 1

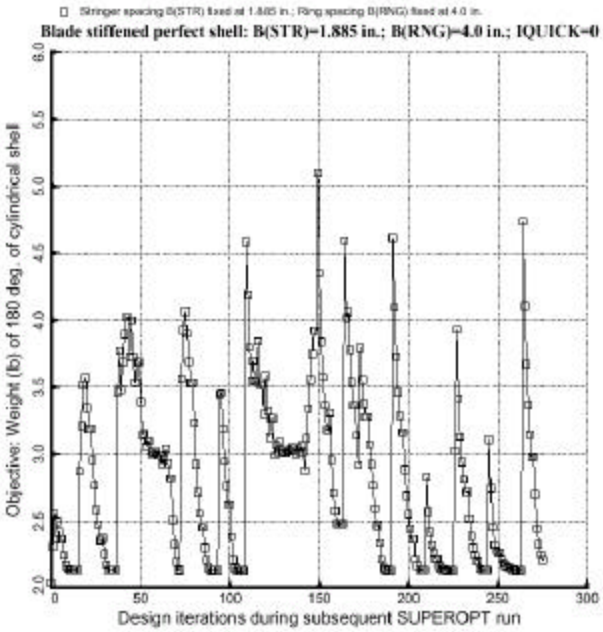

Fig. 9 Objective vs. design iterations from PANDA2 with IQUICK = 0

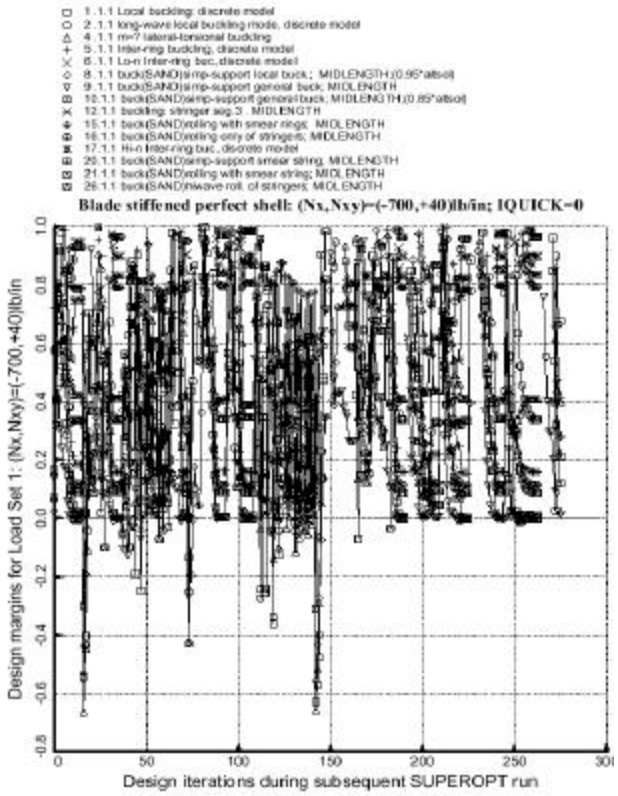

Fig. 10 Margins vs. design iterations from PANDA2 with IQUICK=0

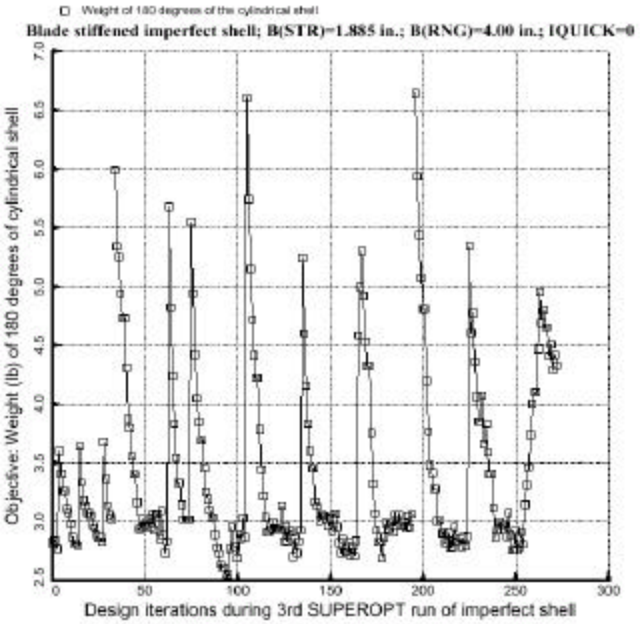

Fig. 11 Objective vs. design iterations from PANDA2 for imperfect Blade stiffened shell

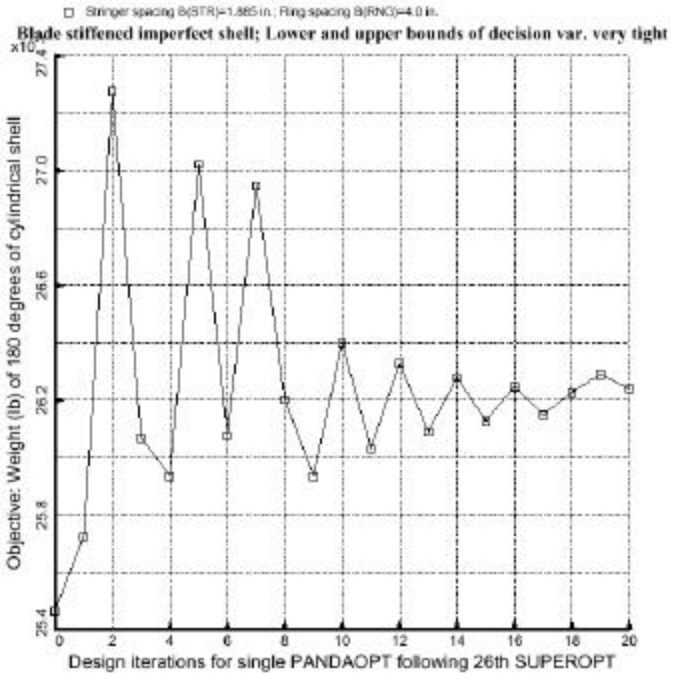

Fig. 12 Objective for near-optimum design of imperfect Blade stiffened shell for which lower and upper bounds of the decision variables have been severely tightened in order to demonstrate oscillatory behavior

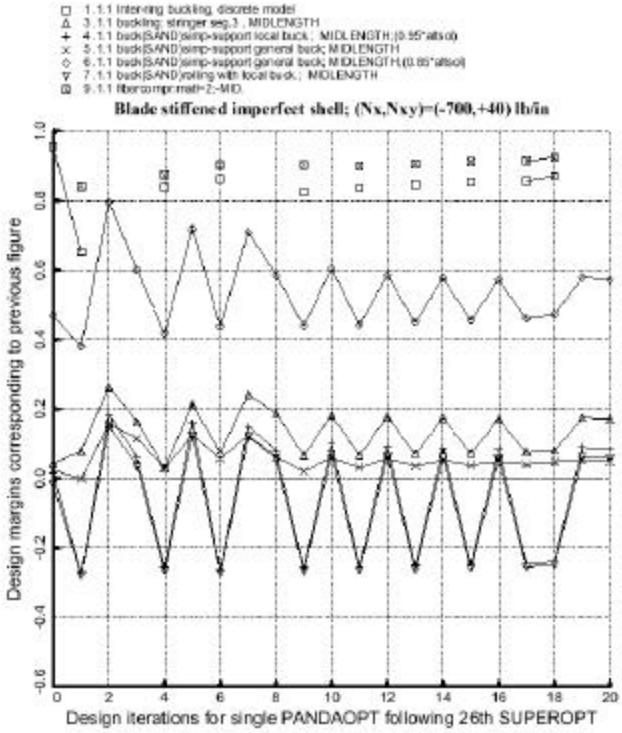

Fig. 13 The margins corresponding in the same case as the previous figure

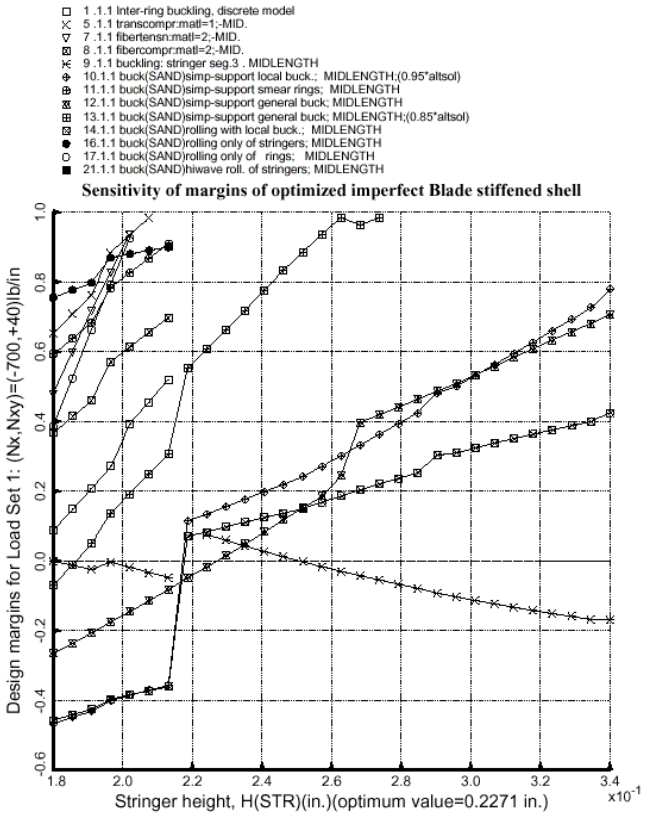

Fig. 14 Margins from design sensitivity run with PANDA2 for the optimized imperfect Blade stiffened shell

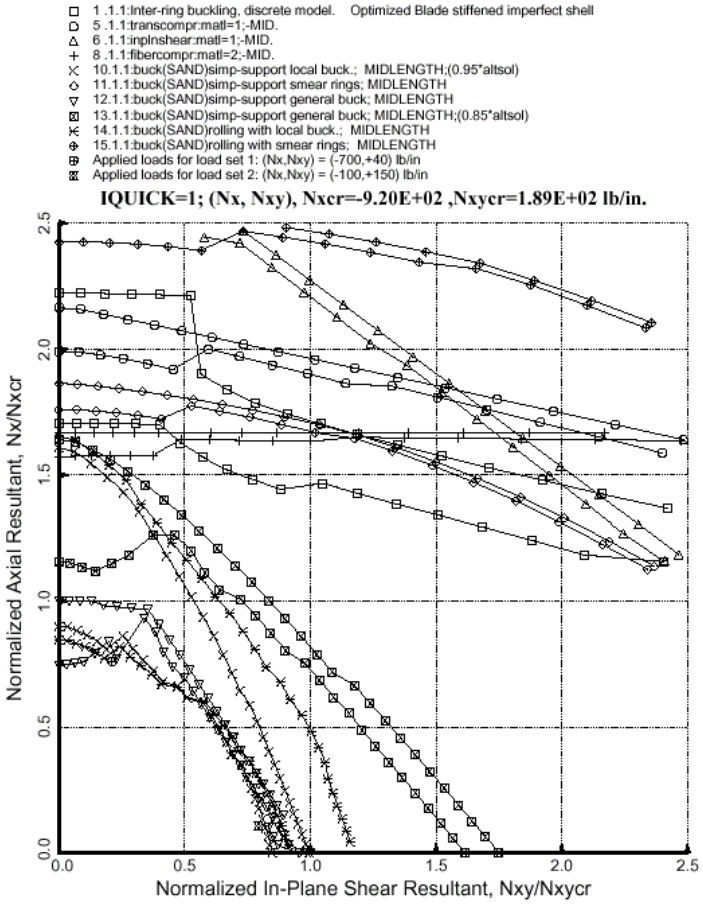

Fig. 15 Load-interaction curves for the optimized imperfect Blade stiffened shell analyzed both as if it were perfect and including the general buckling modal imperfection with amplitude Wimp(general) = 0.025 in.

Fig. 16a First skin buckling mode from STAGS model type “1” with stringer model type “m” and ring model type “s” (Table 13)

Fig. 16b Second skin buckling mode from the same STAGS model as in (a)

Fig. 16c First skin buckling mode in (a) viewed end on, demonstrating that the normal buckling modal displacement w is constant and non-zero along all four edges

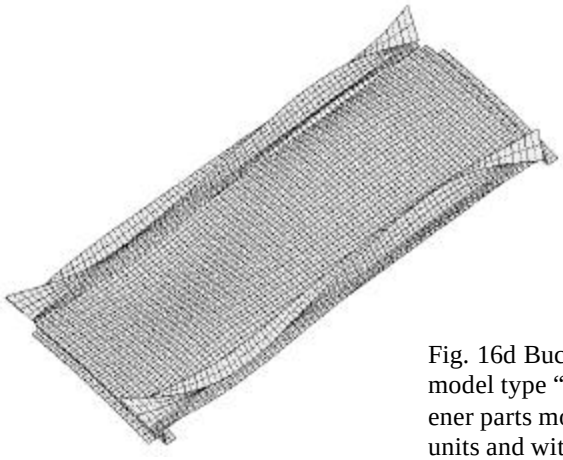

Fig. 16d Buckling in STAGS model type “1” with all stiffener parts modeled as shell units and with stiffener sidesway unrestrained at the edges

Fig. 16e Buckling in same STAGS model as (d) but with stiffener sidesway prevented at the edges

Fig. 16e Buckling in same STAGS model as (e) but with Load Set 2

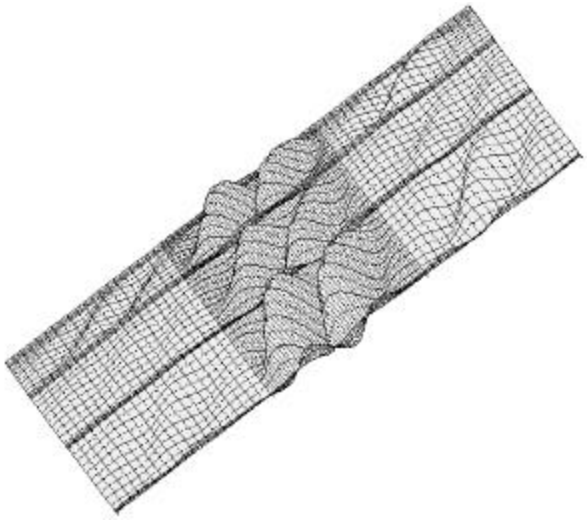

Fig. 17 Buckling of the skin in STAGS model type “2” for optimized perfect Blade stiffened shell

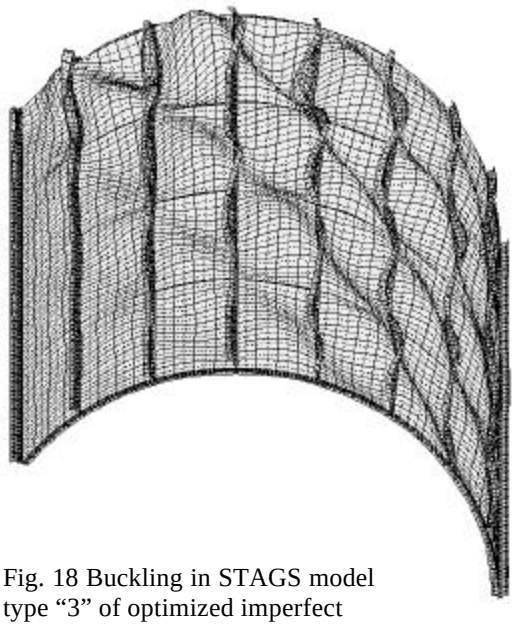

Fig. 18 Buckling in STAGS model type “3” of optimized imperfect Zee stiffened shell

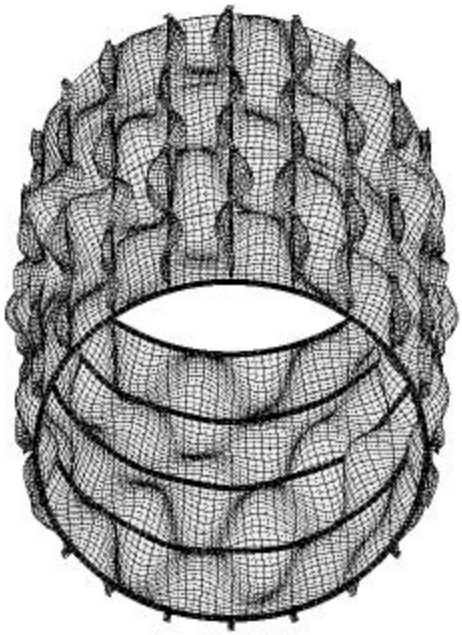

Fig. 19a Buckling in STAGS model type “4” of optimized imperfect Tee stiffened shell

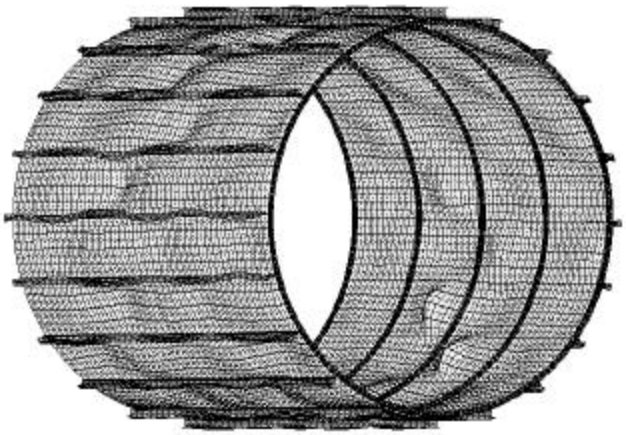

Fig. 19b Mode of collapse of the same shell as shown in Fig. 19a

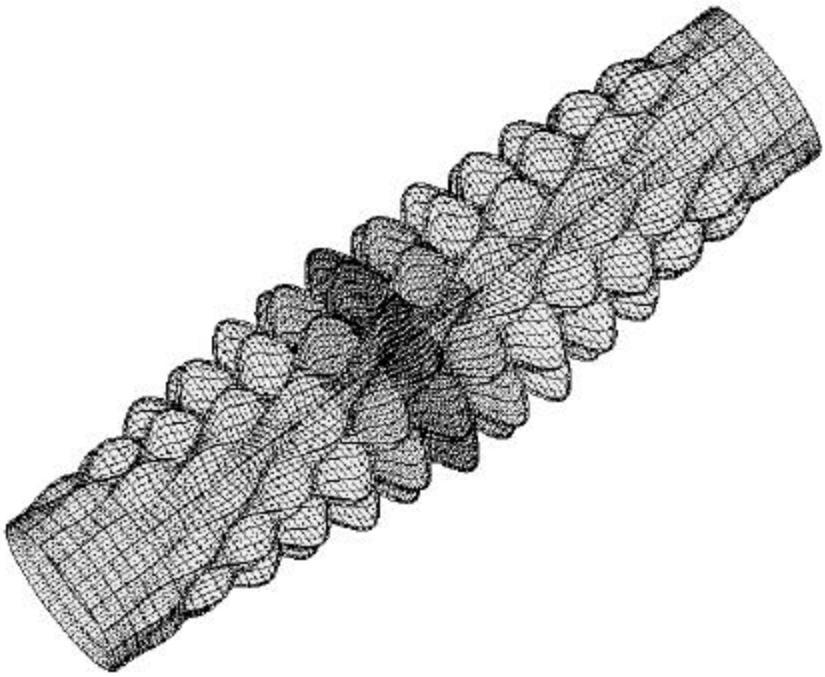

Fig. 20 First buckling mode in STAGS model of type “5” of optimized perfect Blade stiffened shell

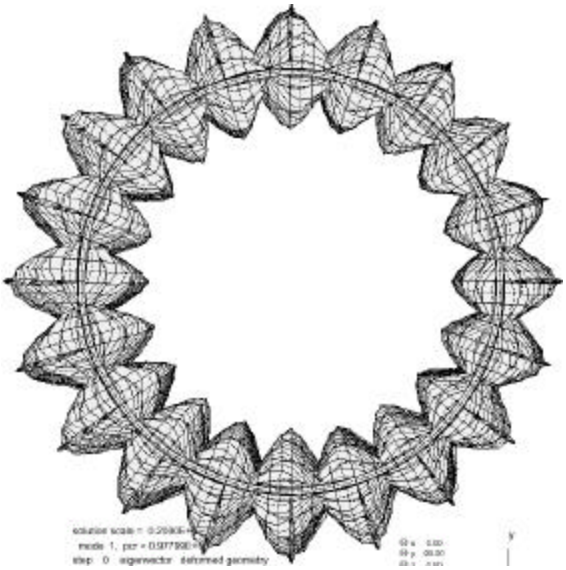

Fig. 21 End view of same buckling mode as shown in Fig. 20

Fig. 22 End view of the same buckling mode as shown in Fig. 20 as experienced by one of the rings nearest to the midlength of the shell

Fig. 23 88th buckling mode of the same shell shown in Fig. 20. This is the lowest buckling mode with a significant component of general instability (n = 3 circumferential waves)

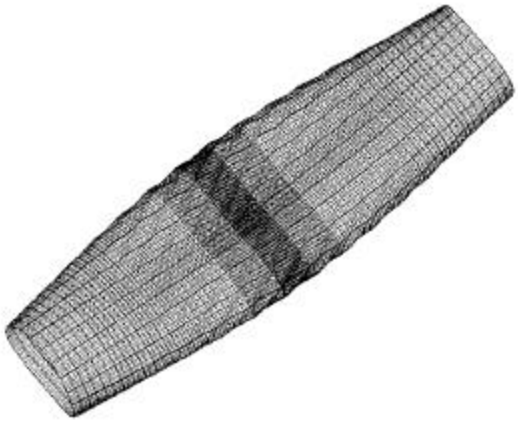

Fig. 24 98th buckling mode of the same shell shown in Fig. 20 (n = 2)

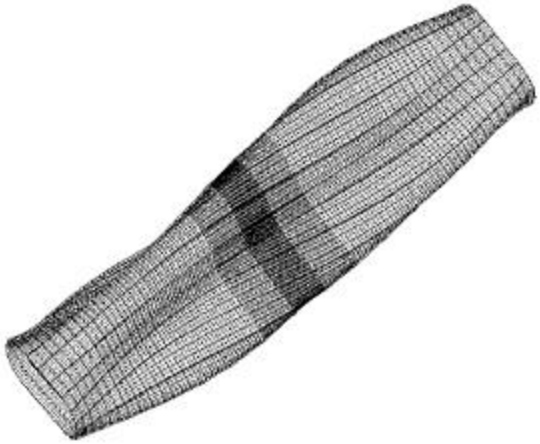

Fig. 25 First buckling mode of optimized imperfect Blade stiffened shell (n = 3)

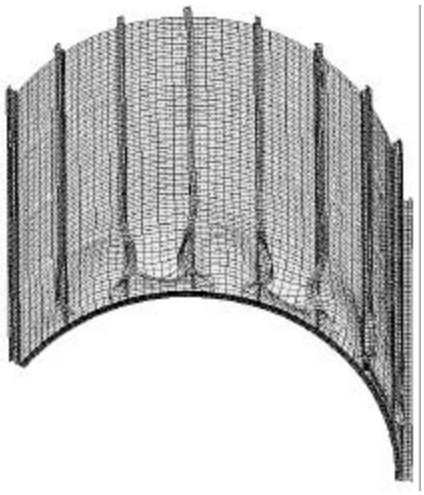

Fig. 26 Collapse mode in STAGS model type "3" for the optimized imperfect Tee stiffened shell in which stiffener sidesway is permitted at the edges

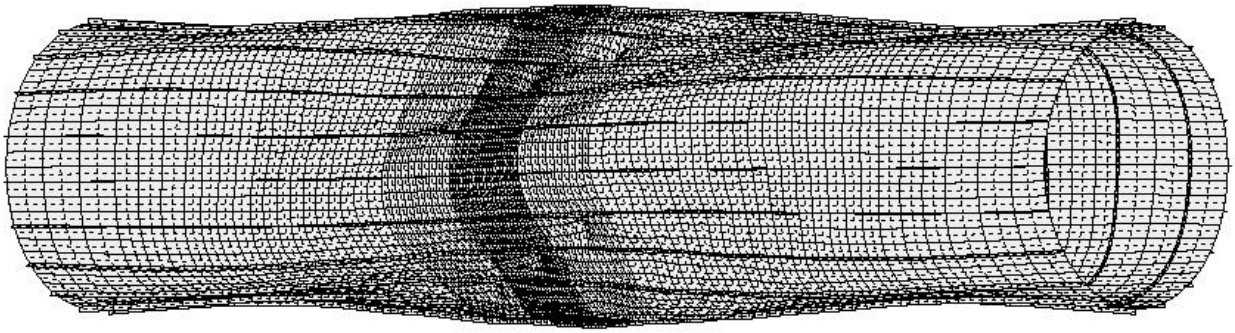

Fig. 27 Collapse mode in STAGS model type "5" for the optimized imperfect Blade stiffened shell

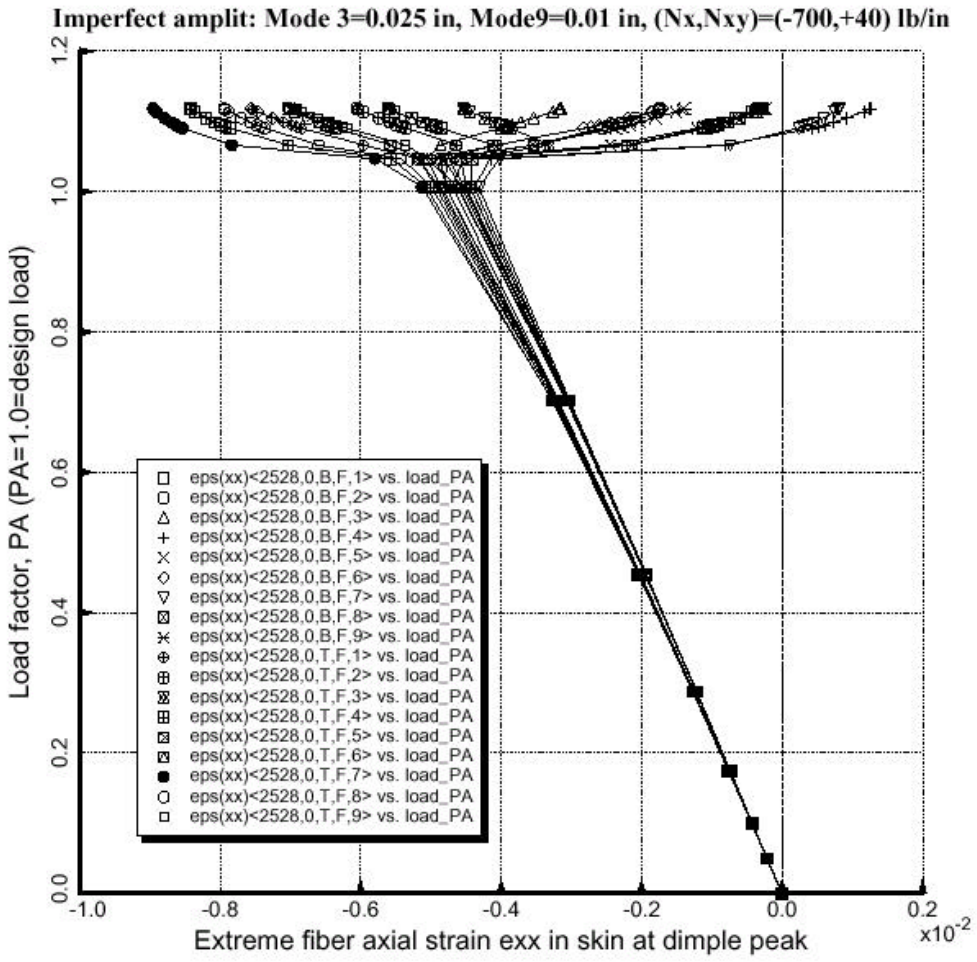

Fig. 28 Extreme fiber axial strain from the nonlinear STAGS analysis of the same shell shown in Fig. 27

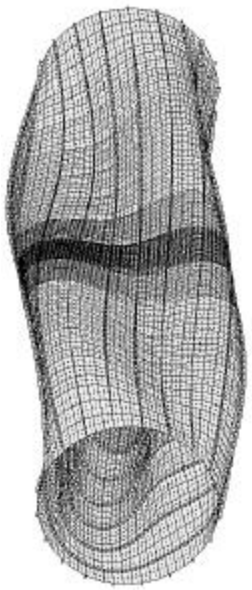

Fig. 29 Collapse mode for the optimized imperfect Blade stiffened shell with initial buckling modal imperfections Wimp (general, n = 3) = 0.025 in. and Wimp (panel, Fig. 20) = 0.0001 in.

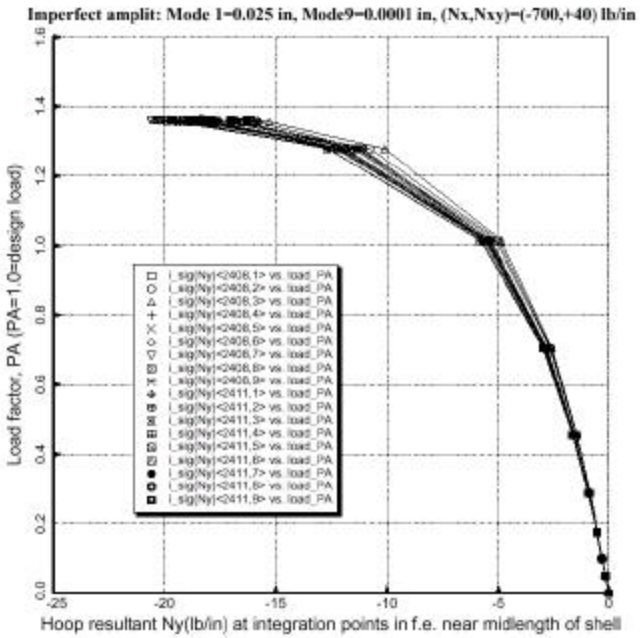

Fig. 30 Hoop compression at integration points in finite elements in center of band near midlength of shell shown in Fig. 29, where nodal point density is highest and imperfection-induced hoop compression in the skin is maximum.

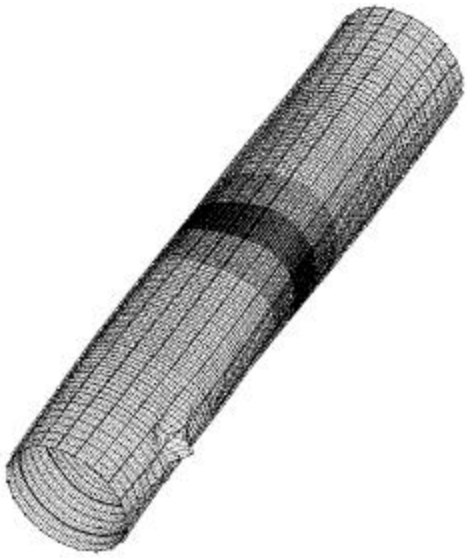

Fig. 31 Lowest buckling mode from the nonlinear STAGS run at load factor 1.361. The shell is deformed as shown in Fig. 29.

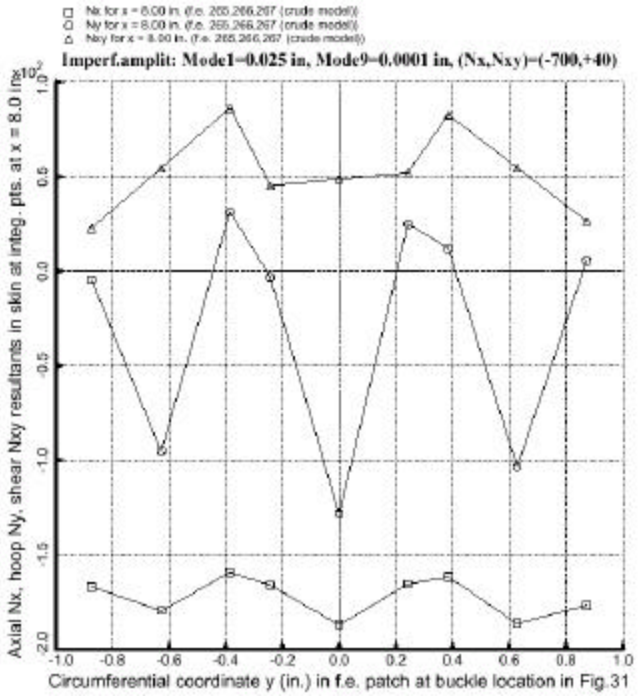

Fig. 32 Values of stress resultants at the integration points in a finite element patch where local buckling is shown to occur in Fig. 31

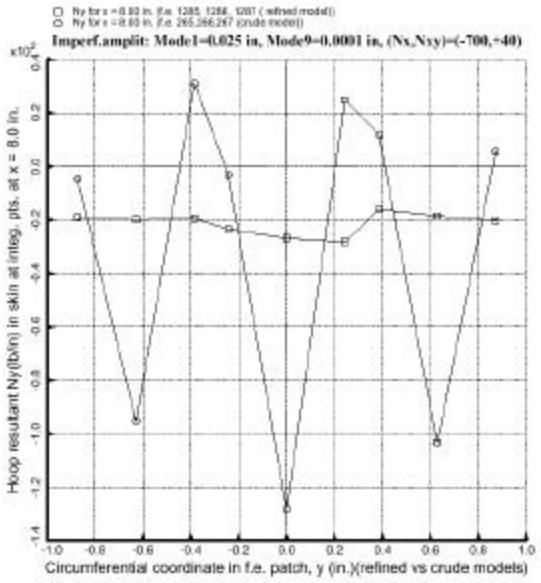

Fig. 33 Hoop resultants at integration points at the location where local buckling occurs as shown in Fig. 31 from models with sparse and dense nodal point meshes

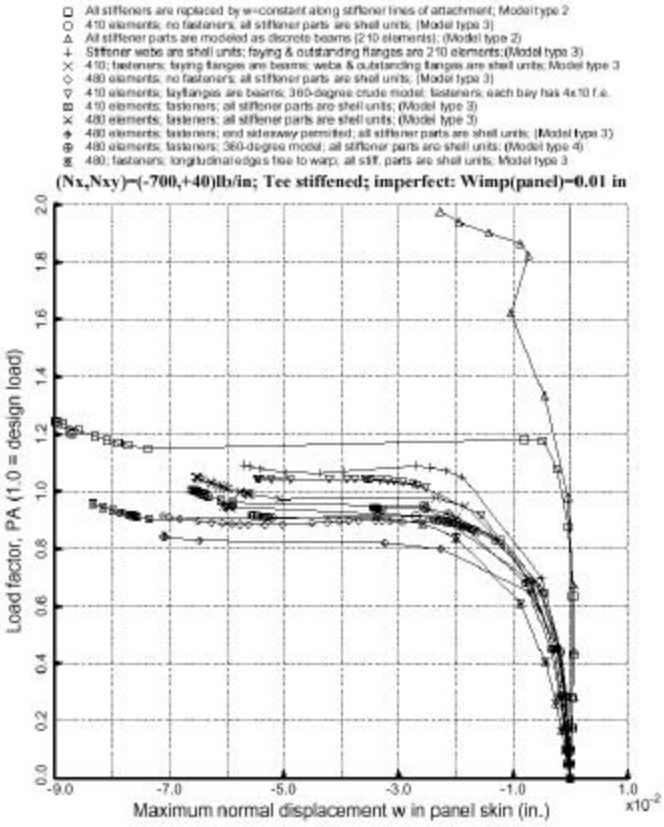

Fig. 34 Load-deflection curves from several STAGS models of the optimized imperfect Tee stiffened shell

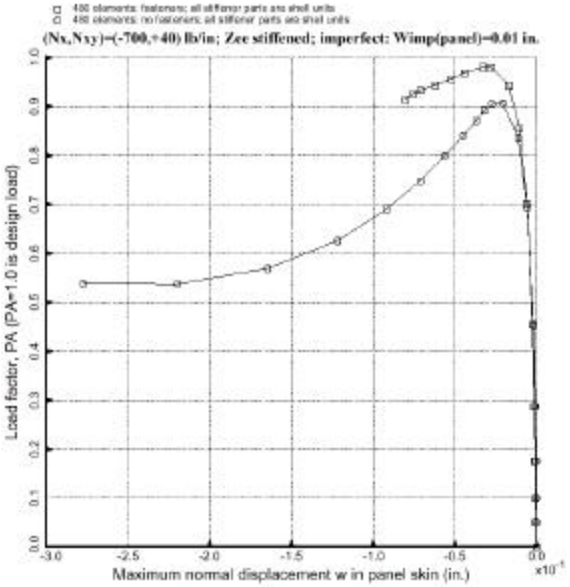

Fig. 35 Collapse of optimized imperfect Zee stiffened shell with and without fasteners used in the STAGS model

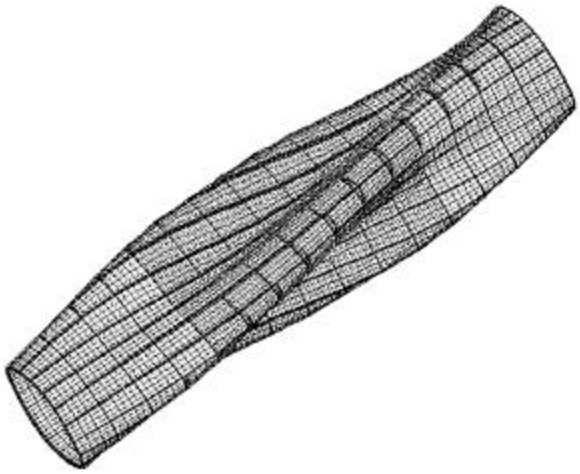

Fig. 36 The first general buckling mode from STAGS model type “5” of optimized imperfect Zee stiffened shell

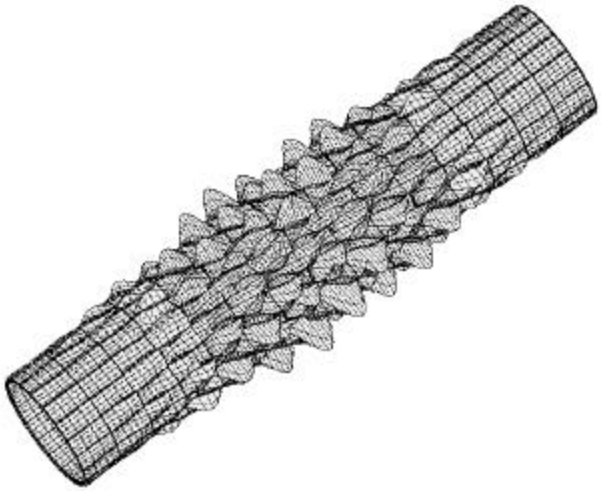

Fig. 37 The first buckling mode from the same STAGS model as shown in Fig. 36

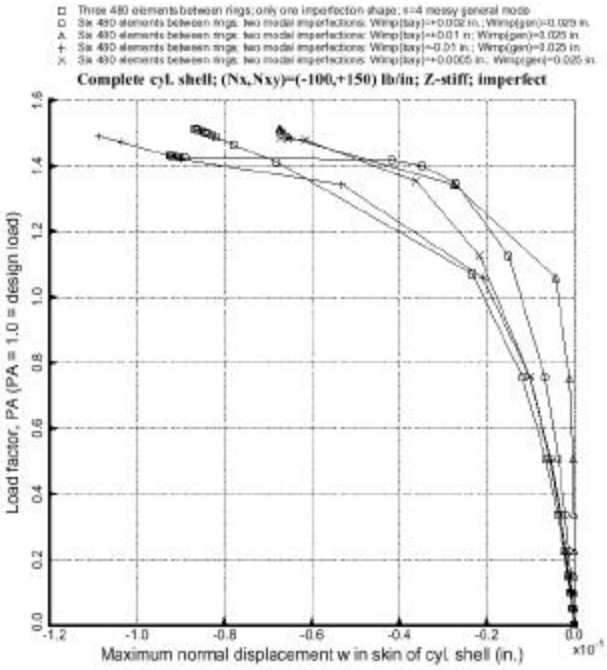

Fig. 38 Collapse of optimized imperfect Zee stiffened shells from STAGS model shown in Figs. 36 and 37

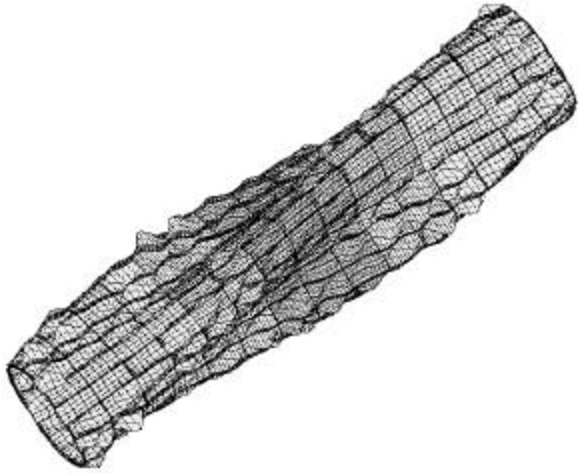

Fig. 39 A general buckling mode for the optimized imperfect Zee stiffened shell. The mode is too “polluted” by local buckling to use as a general buckling modal imperfection.

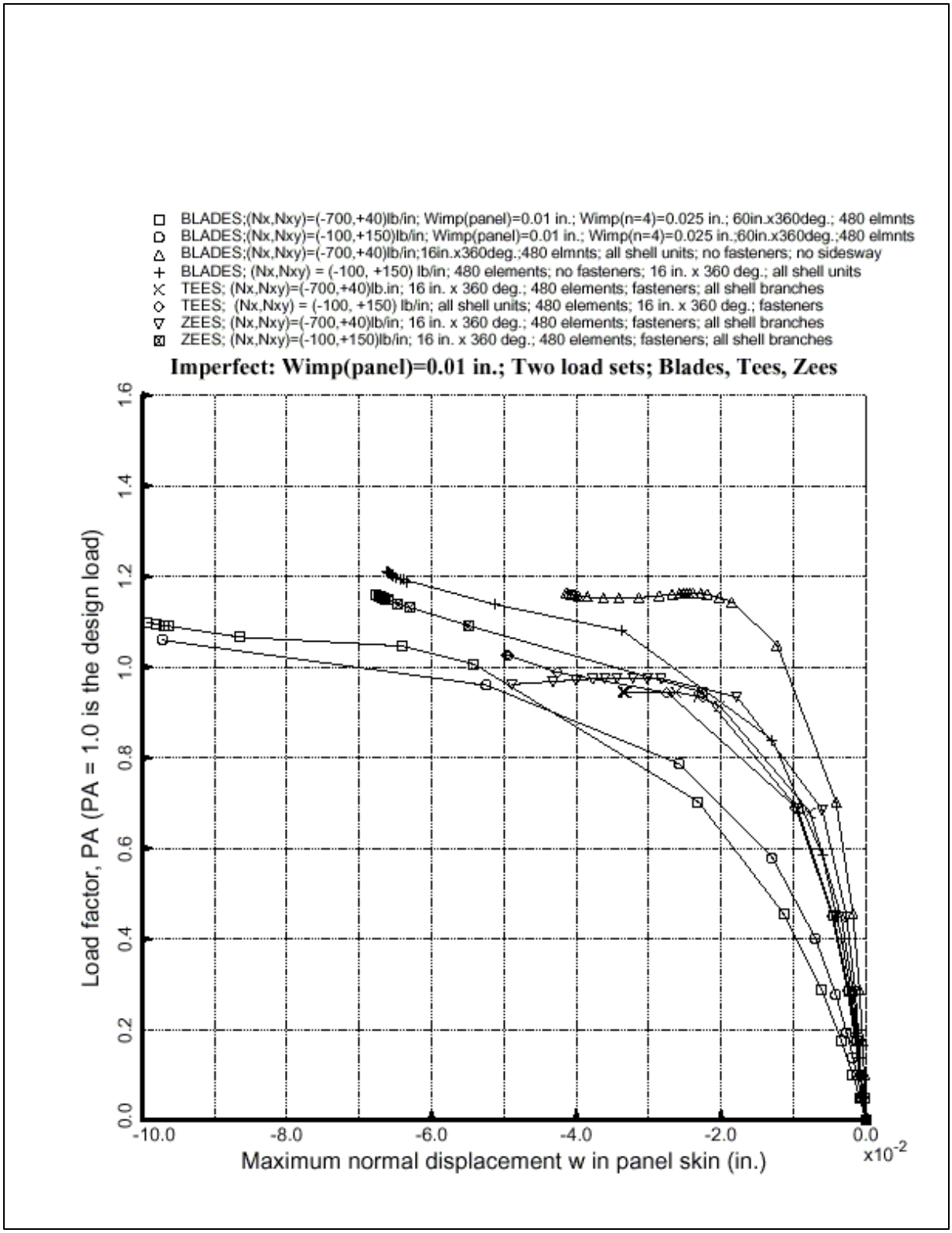

Fig. 40 Collapse of optimized imperfect Blade, Tee and Zee stiffened cylindrical shells